Available online at www.sciencedirect.com

ScienceDirect

Geochimica et Cosmochimica Acta 126 (2014) 371–397

Geochimica et Cosmochimica Acta

www.elsevier.com/locate/gca

Carbonation rates of peridotite in the Samail Ophiolite, Sultanate of Oman, constrained through ^{14}C dating and stable isotopes

Evelyn M. Mervine [a,*], Susan E. Humphris [b], Kenneth W.W. Sims [c], Peter B. Kelemen [d], William J. Jenkins [e]

[a] MIT/WHOI Joint Program, Geology and Geophysics Department, Woods Hole Oceanographic Institution, 266 Woods Hole Road, Woods Hole, MA 02543, USA
[b] Geology and Geophysics Department, Woods Hole Oceanographic Institution, 266 Woods Hole Road, Woods Hole, MA 02543, USA
[c] Geology and Geophysics Department, University of Wyoming, 1000 East University Avenue, Laramie, WY 82071, USA
[d] Lamont-Doherty Earth Observatory, 61 Route 9W, Palisades, NY 10964, USA
[e] Marine Chemistry and Geochemistry Department, Woods Hole Oceanographic Institution, 266 Woods Hole Road, Woods Hole, MA 02543, USA

Received 25 June 2013; accepted in revised form 7 November 2013; Available online 20 November 2013

Abstract

Detailed ^{14}C dating as well as stable C and O isotope analyses were conducted on carbonates formed during alteration of the peridotite layer of the Samail Ophiolite, Sultanate of Oman. ^{14}C results obtained in this and previous studies indicate that surface travertines range in age from modern to >45,000 yr BP, indicating long-term deposition and preservation. Travertine deposition rates in two localities were ~0.1 to 0.3 mm/yr between ~30,000 and 45,000 yr BP. Using an estimate of total travertine area, this would result in a maximum of ~1000 to 3000 m^3/yr of travertine being deposited throughout the ophiolite during this time period. This travertine deposition would have sequestered a maximum of ~1 to 3 × 10^6 kg CO$_2$/yr. Ca-rich carbonate veins that are associated with the surface travertine deposits have ages ranging from ~4000 to 36,000 yr BP (average: 15,000 yr BP). Mg-rich carbonate veins exposed in outcrops have ages ranging from ~8000 to 45,000 yr BP (average: 35,000 yr BP). Detailed sampling from numerous locations (3 locations in this study and 10 locations in the previous studies) indicates that no carbonate veins from the natural peridotite weathering surface are older than the ~50,000 yr BP dating limit of ^{14}C. However, ^{14}C dating of Mg-rich carbonate veins from three roadcut exposures (Qafeefah, Fanja, and Al-Wuqbah) indicates that a significant number of roadcut veins are ^{14}C dead (>50,000 yr BP). A location weighted average indicates that ~40% of veins sampled at the three roadcuts are ^{14}C dead. An average including veins sampled at both roadcuts and outcrops indicates that overall ~8% of Mg-rich carbonate veins are ^{14}C dead. Mg-rich carbonate veins are estimated to sequester on the order of 10^7 kg CO$_2$/yr throughout the ophiolite.

1. INTRODUCTION

The formation of carbonate minerals as alteration products in mafic and ultramafic rocks is a poorly constrained sink in the global carbon cycle (e.g. Staudigel et al., 1989; Alt and Teagle, 1999; Dessert et al., 2001, 2003; Wilson et al., 2006, 2009a,b; Goldberg et al., 2008; Kelemen and Matter, 2008; Matter and Kelemen, 2009; Kelemen et al.,

---

* Corresponding author. Present address: AuruMar (Pty.) Ltd., DBM Gardens, Golf Park 2, Raapenberg Road, Pinelands, 7405 Cape Town, South Africa. Tel.: +27 (0)21 658 3224.
E-mail addresses: emervine@whoi.edu, evelyn.mervine@aurumar.co.za (E.M. Mervine), shumphris@whoi.edu (S.E. Humphris), ksims7@uwyo.edu (K.W.W. Sims), peterk@ldeo.columbia.edu (P.B. Kelemen), wjenkins@whoi.edu (W.J. Jenkins).

0016-7037/$ - see front matter © 2013 Elsevier Ltd. All rights reserved.
http://dx.doi.org/10.1016/j.gca.2013.11.007

2011). While mafic rocks are more abundant than ultramafic rocks on Earth's surface, ultramafic rocks likely have faster carbonation rates than mafic rocks (O'Connor et al., 2004; Chizmeshya et al., 2007; Matter and Kelemen, 2009; Kelemen et al., 2011). Furthermore, studies of fully carbonated peridotites, which are known as "listvenites", show that under certain conditions ultramafic rocks take up significantly more CO_2 per kg than mafic rocks (e.g. Halls and Zhao, 1995; Hansen et al., 2005; Akbulut et al., 2006; Nasir et al., 2007; Boschi et al., 2009; Kelemen et al., 2011; Beinlich et al., 2012).

While natural carbonation of uplifted peridotite is commonly observed subaerially and on the seafloor (e.g. Trommsdorff and Evans, 1977; Trommsdorff et al., 1980; Ferry, 1995; Surour and Arafa, 1997; Kelley et al., 2001; Früh-Green et al., 2003; Ludwig et al., 2006, 2011; Kelemen and Matter, 2008; Matter and Kelemen, 2009; Power et al., 2009; Kelemen et al., 2011; Pronost et al., 2011; Beinlich and Austrheim, 2012; Harrison et al., 2013), the natural rate of peridotite carbonation and therefore the rate of CO_2 uptake via this alteration mechanism is poorly constrained (e.g. Wilson et al., 2006, 2009a,b; Kelemen and Matter, 2008; Kelemen et al., 2011). Determining the natural peridotite carbonation rate is critical for understanding the role of this potentially important sink in the global carbon cycle and is also an essential, but poorly constrained, parameter in calculations evaluating the viability of using artificially-enhanced, *in situ* alteration of peridotite to mitigate the buildup of anthropogenic CO_2 in the atmosphere (e.g. Seifritz, 1990; Lackner et al., 1995; Lackner, 2002; Kelemen and Matter, 2008; Matter and Kelemen, 2009; Kelemen et al., 2011).

An excellent location for investigating natural rates of carbonate formation in peridotite is the Samail Ophiolite, Sultanate of Oman, where abundant carbonate veins as well as calcite-rich travertines are found throughout the peridotite (e.g. Neal and Stanger, 1984, 1985; Clark and Fontes, 1990; Clark et al., 1992; Kelemen and Matter, 2008; Kelemen et al., 2011). Previous work has suggested that the veins have an average age of ~26,000 ± 12,000 (1σ SD) yr BP with 2 samples older than the ~50,000 yr BP, the age limit of the ^{14}C dating technique (Kelemen and Matter, 2008; Kelemen et al., 2011). In this paper we present detailed ^{14}C dating as well as stable C and O isotope data for carbonates sampled at eight field locations in order to further assess rates of natural carbonation of Samail Ophiolite peridotite.

2. GEOLOGIC SETTING

The Samail Ophiolite (Fig. 1) is one of the largest and best exposed ophiolites in the world and is part of a chain of related ophiolites found along the northern part of the Arabian plate. The Samail Ophiolite consists of several uplifted, thrust-bounded blocks (nappes) of oceanic crust and mantle that were obducted at ~80 to 95 Ma on top of autochthonous shelf carbonate rocks (the Hajar Supergroup) and parautochthonous continental slope carbonate rocks (the Sumeini Group), which rest on top of pre-Permian crystalline basement (Glennie et al., 1973, 1974; Coleman, 1981; Lippard et al., 1986; Searle and Cox, 1999, 2002). These nappes consist of ~47 km of crustal rocks (layered gabbros, sheeted dikes, and volcanics, including pillow lavas) and ~8 to 12 km of upper mantle, primarily harzburgite (Glennie et al., 1973, 1974; Coleman, 1981; Lippard et al., 1986; Nicolas et al., 2000). The ophiolite is ~50 to 100 km wide and extends for at least 500 km (Coleman, 1981; Nicolas et al., 2000).

Low-temperature alteration of peridotite in the Samail Ophiolite has been proposed to occur in three steps, as shown in Fig. 2 (Barnes et al., 1967, 1978; Barnes and O'Neil, 1969; Neal and Stanger, 1985; Bruni et al., 2002; Cipolli et al., 2004; Kelemen et al., 2011; Paukert et al., 2012). In the first step, meteoric water weathers partially serpentinized peridotite in equilibrium with the atmosphere, forming Mg^{2+}–HCO_3^- rich waters known as "Type I" waters. In the second step, these waters percolate deeper into the peridotite bedrock and are isolated from the atmosphere. These deeper waters precipitate Mg-rich carbonates, such as magnesite and dolomite, and serpentine and clay are also formed. Precipitation of these minerals leads to an increase in Ca^{2+} in the fluid since Ca is largely excluded from these alteration minerals. Ca^{2+}-rich waters, known as "Type II" waters, are depleted in magnesium and carbon and have pH of 10 to 12 and an Eh of approximately −200 mV (Neal and Stanger, 1983, 1984, 1985; Clark and Fontes, 1990; Paukert et al., 2012). In the third step, the Type II waters return to the surface as hyperalkaline springs, where they rapidly take up atmospheric CO_2 and precipitate abundant, calcite-rich travertine.

This study focuses on two types of carbonate formed during this alteration process. The first type is calcite-rich travertines (Fig. 3) precipitated from high pH (values of 10 to 12) springs found throughout the ophiolite (e.g. Neal and Stanger, 1984, 1985; Clark and Fontes, 1990; Clark et al., 1992; Kelemen and Matter, 2008; Kelemen et al., 2011; Paukert et al., 2012). These springs are predominantly located in the peridotite layer and are concentrated along the basal thrust of the ophiolite as well as at the crust-mantle boundary (Neal and Stanger, 1984, 1985; Dewandel et al., 2003, 2004, 2005). Thick travertine deposits (up to several meters, on average 1 to 2 m) form on top of peridotite, which is highly fractured with abundant carbonate-serpentine veins. Turquoise-blue hyperalkaline pools lined with white carbonate precipitate are a feature of many alkaline springs. Browner, more weathered (and presumably older) travertine deposits are often found upslope and to the side of the actively precipitating travertine deposits. Kelemen and Matter (2008) estimate that there are ~45 large travertine deposits in the entire Samail Ophiolite and that these deposits represent ~10^7 m^3 of exposed travertine. Furthermore, based on measurements in outcrops immediately underlying travertine, they estimate that the travertine deposits are underlain by a ~10 m thick peridotite layer with ~5% Ca-rich carbonate veins, so the total volume of carbonate associated with the travertine deposits is probably 2.5 times the exposed volume.

The second type of carbonate analysed in this study is carbonate veins (Fig. 3, Panel D and Fig. 4) that form *in situ* in the peridotite and, to a lesser extent, in the gabbro and basalt layers of the ophiolite (Kelemen and Matter, 2008; Kelemen et al., 2011). Carbonate veins adjacent to

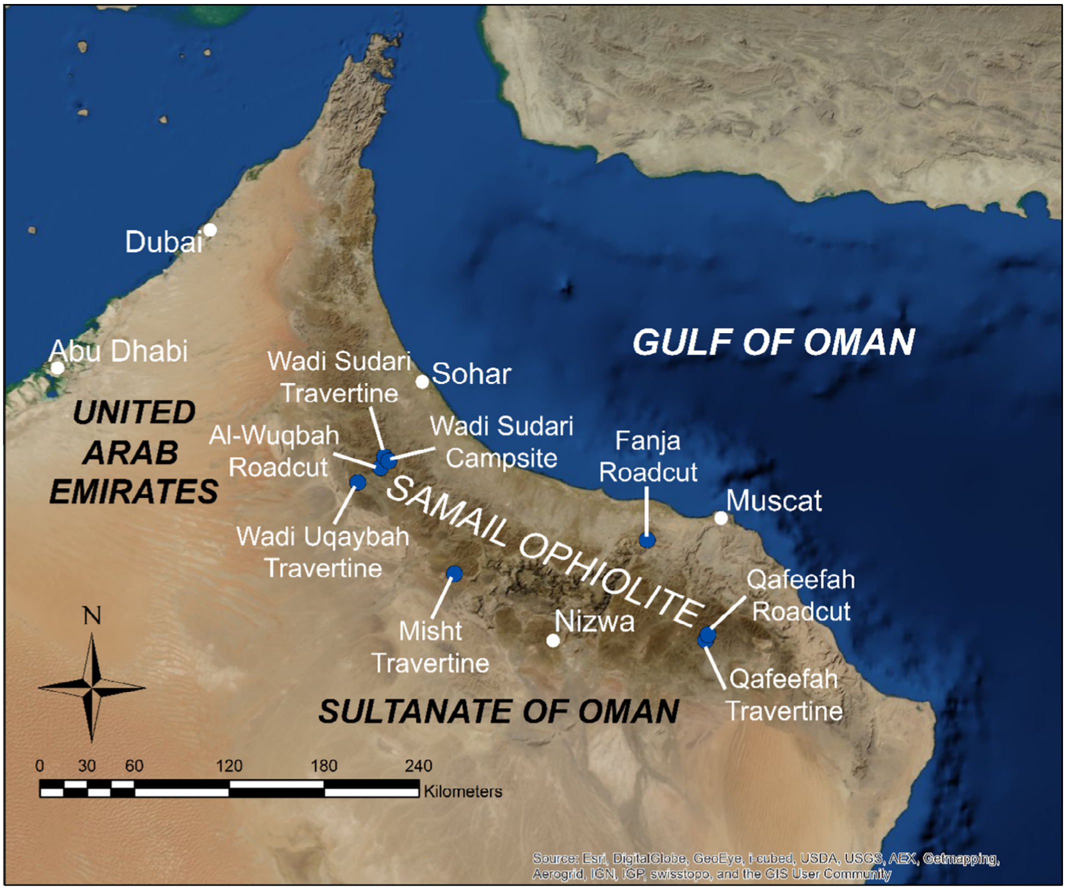

Source: Esri, DigitalGlobe, GeoEye, i-cubed, USDA, USGS, AEX, Getmapping, Aerogrid, IGN, IGP, swisstopo, and the GIS User Community

Fig. 1. The eight field locations (blue circles) where carbonate and peridotite samples were collected in the Samail Ophiolite during 2009 and 2010 field seasons. Map made using ArcGIS, Version 10.1. (For interpretation of the references to color in this figure legend, the reader is referred to the web version of this article.)

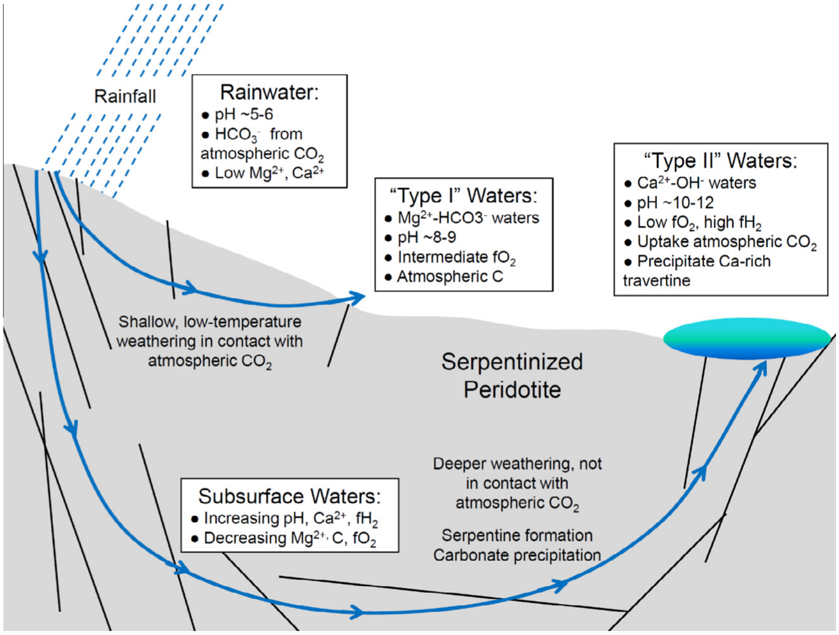

Fig. 2. Schematic illustrating the behavior of CO_2 in Type I and Type II waters associated with alteration of partially-serpentinized peridotite. Figure modified from Neal and Stanger (1985).

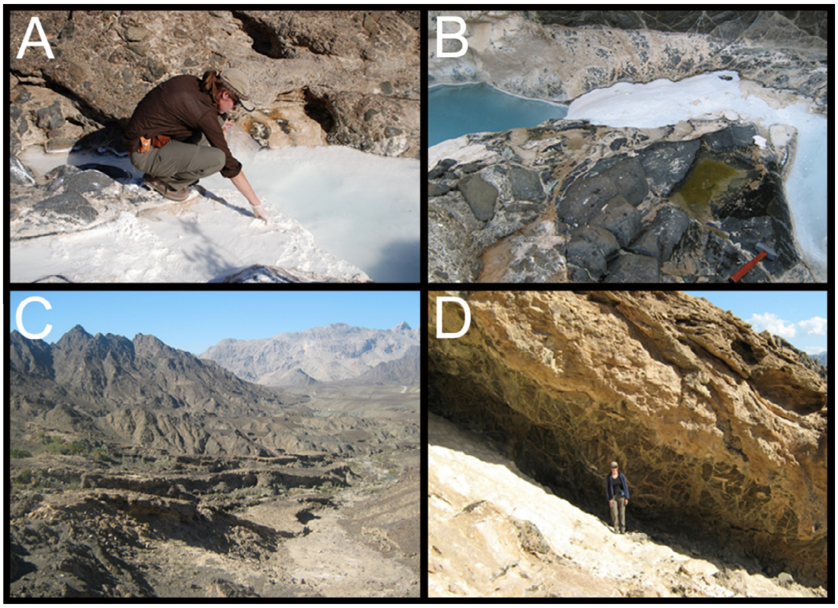

Fig. 3. Representative images of calcite-rich travertines in the peridotite layer of the Samail Ophiolite. A: Recently-formed carbonate precipitate in a hyperalkaline streambed at Qafeefah Travertine. B: A turquoise alkaline pool and recently-formed carbonate precipitate at Wadi Sudari Travertine. Note the hammer for scale. C: Brown, fossil travertine terraces at Wadi Uqaybah Travertine. The travertine terraces are ~1 to 2 m thick and are found extensively throughout the wadi. Note how the terraces are broken by incised channels, which are filled with lighter colored travertines. Many of the incised channels also contain hyperalkaline pools and seeps. D: Calcite-rich travertine veins exposed in peridotite underneath a thick fossil travertine deposit at Wadi Sudari Travertine. (For interpretation of the references to color in this figure legend, the reader is referred to the web version of this article.)

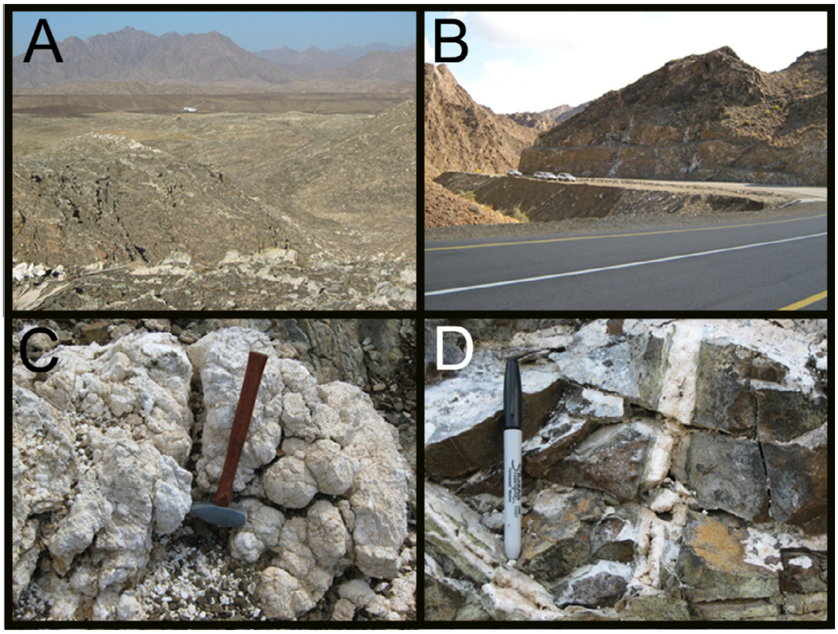

Fig. 4. Representative images of Mg-rich carbonate veins exposed on the natural peridotite weathering surface (A and C) and at roadcuts (B and D) in the Samail Ophiolite. A: Bright white magnesite veins exposed in outcrop on the natural peridotite weathering surface at Wadi Sudari Campsite. B: Magnesite, dolomite, and gabbro veins exposed on a roadcut through peridotite near the town of Fanja. Note the Land Cruisers for scale. C: A white magnesite vein with botryoidal texture exposed on the natural peridotite weathering surface near to Fanja Roadcut. Note the hammer for scale. D: Dolomite-serpentine veins exposed on the surface of Fanja Roadcut. Note the Sharpie marker for scale. (For interpretation of the references to color in this figure legend, the reader is referred to the web version of this article.)

surface travertine deposits are Ca-rich and similar in composition to the travertines. Carbonate veins sampled far from travertines are generally Mg-rich and presumably formed in the deeper subsurface during the transformation of Type I waters to Type II waters. The Mg-rich carbonate veins are predominately composed of magnesite and dolomite, range in size from a few millimeters to several meters thick, and can extend for hundreds of meters (Kelemen and Matter, 2008; Kelemen et al., 2011). The Mg-rich carbonate veins are often encompassed by or intergrown with serpentine veins. Based on data gathered at newly formed roadcuts, Kelemen and co-workers estimate that carbonate veins comprise ~1% of near-surface peridotite in the Samail Ophiolite (Kelemen and Matter, 2008; Kelemen et al., 2011).

3. SAMPLE DESCRIPTIONS

Sample descriptions are given in Table 1. A total of 55 carbonate samples were collected from four locations of travertine deposition: Qafeefah[1] Travertine, Misht Travertine, Wadi Uqaybah Travertine, and Wadi Sudari Travertine (Fig. 1). These sites are located in the peridotite layer of the ophiolite and were selected on the basis of catchment geometry (catchments in peridotite and, in some cases, also gabbro) to minimize the possibility that dissolution of older limestone proximal to the ophiolite contributes Ca and C to the travertines.

Actively forming carbonate precipitates were collected from the surfaces and bottoms of hyperalkaline pools (Fig. 3, Panels A and B). These samples are distinguished as "recently-formed travertine precipitates". Travertine was also collected from ~1 to 2 m thick travertine terraces ("travertine terraces") and from younger travertine in incised channels located between older terrace formations ("channel-filling terraces") (Fig. 3, Panels C and D). In order to estimate rates of travertine deposition, at least five distinct layers of a ~2 m thick travertine terrace were subsampled at Misht Travertine, and two ~1 m thick terraces were subsampled at Wadi Uqaybah Travertine.

At many travertine locations, stalactite- and stalagmite-like travertine formations (distinguished as "pseudospeleothems") have developed in overhangs, such as underneath terrace formations. Note that these features are not true speleothems because they were not formed within caves. Two pseudospeleothem formations were sampled at Wadi Sudari. One sample was a pseudospeleothem that was observed to be actively forming from a drip originating from an overhanging travertine terrace. The other sample is a layered pseudospeleothem that was collected from a pile of pseudospeleothem "drops" that had fallen from a travertine overhang. Subsampling of this layered pseudospeleothem was conducted in order to determine rates of travertine pseudospeleothem growth.

A total of 31 samples were collected from three roadcuts exposing carbonate veins (Qafeefah Roadcut, Fanja Roadcut, and Al-Wuqbah Roadcut) and from one campsite located on the natural peridotite weathering surface (Wadi Sudari Campsite) (Fig. 1). For the purposes of this study, we distinguish three types of carbonate veins (Fig. 3, Panel D and Fig. 4). "Travertine veins" are Ca-rich (calcite or dolomite) veins that were sampled within ~1 to 10 m of surface travertine deposits (Fig. 3, Panel D). Mg-rich carbonate veins are divided into "outcrop veins" (sampled from the natural peridotite weathering surface; Fig. 4, Panels A and C) and "roadcut veins" (sampled at roadcuts, Fig. 4, Panels B and D). The roadcut veins are generally less weathered than the outcrop veins, which are often partially eroded.

4. METHODS

Selected carbonate veins and travertines were crushed in a jaw crusher and then purified using magnetic separation and handpicking. Many of the carbonate veins consist of multiple minerals (e.g. magnesite, calcite, dolomite, and serpentine). Whenever possible, monomineralic (or nearly so) separates were prepared, and their purity was evaluated by powder X-ray diffraction (XRD) analysis at Woods Hole Oceanographic Institution using a Philips Analytical PW1830 XRD machine. Mineral identification was conducted using the International Center for Diffraction Data Powder Diffraction File.

The travertine terraces and pseudospeleothems are often finely laminated, heterogeneous on small length scales, and contain crosscutting carbonate veins. Previous studies have indicated that a few centimeters of travertine can represent several hundreds to thousands of years of travertine deposition (Clark and Fontes, 1990; Kelemen and Matter, 2008; Kelemen et al., 2011). Hence, the samples were carefully subsampled on a ~1 mm scale by milling ~50 to 100 mg of carbonate material from rock slabs using a semi-automated microsampler (see methods in Vadpalas et al., 2011).

All ^{14}C dating was conducted at the National Ocean Sciences Accelerator Mass Spectrometry Facility (NOSAMS) at Woods Hole Oceanographic Institution. For each sample, ~10 to 50 mg of handpicked or microsampled carbonate was weighed out for analysis. Immediately prior to dissolution, the samples were etched in 10% hydrochloric acid at room temperature to remove modern atmospheric CO_2 adsorbed on mineral surfaces. Samples comprised primarily of calcite, dolomite, or aragonite were etched for 20 to 30 s until approximately 50% of the material had dissolved. Samples comprised primarily of magnesite dissolved more slowly, so these samples were etched in 10% hydrochloric acid for several minutes until at least 10% of the material had dissolved.

The etched carbonate samples were dissolved in concentrated phosphoric acid on a vacuum line, and CO_2 gas was extracted using cryogenic traps. The CO_2 was converted to graphite using either the standard acid dissolution method (Vogel et al., 1987; McNichol et al., 1995) or the sealed tube graphitization method (Xu et al., 2007; Burke et al., 2010).

---

[1] Due to inconsistencies in transliteration from Arabic to English, Qafeefah has previously been spelled "Khafifah" or "Khafeefah" on maps and in geologic literature since at least 1981 (e.g. Pallister and Hopson, 1981; Kelemen and Matter, 2008). However, a more correct transliteration is "Qafeefah", which is consistent with some but not all road signs. Paukert et al. (2012) refer to the same location as "Qafifah".

Table 1
Sample locations and descriptions.

Sample name	Location	UTM-Easting	UTM-Northing	Description	Major minerals (XRD)	Minor minerals (XRD)
Travertines						
OM09-27C-MS	Qafeefah Travertine	0646207	2533711	Travertine terrace	Calcite	Chrysotile, kaolinite, other unidentified clay
OM09-31C-MS	Qafeefah Travertine	0646222	2533888	Travertine terrace	Calcite	Unidentified clay
OM09-32C-MS-WHITE	Qafeefah Travertine	0646145	2533666	Travertine terrace	Calcite	Unidentified clay
OM09-32C-MS-BROWN	Qafeefah Travertine	0646145	2533666	Travertine terrace	Calcite, dolomite	Kaolinite, other unidentified clay
OM09-33C-MS	Qafeefah Travertine	0646144	2533672	Travertine vein	Calcite	Dolomite, aragonite, chrysotile, unidentified clay
OM09-28C-MS	Qafeefah Travertine	0646210	2533807	Channel-filling travertine	Calcite	Unidentified clay
OM09-6COPS-MS	Qafeefah Travertine	0646107	2533645	Recently-formed travertine precipitate	Aragonite	Calcite, hydromagnesite?, spinel?, unidentified clay
OM09-7COPS-MS	Qafeefah Travertine	0646107	2533645	Recently-formed travertine precipitate	Aragonite	Brucite, calcite, spinel?, unidentified clay
OM10-1COPS-MG	Qafeefah Travertine	0646117	2533648	Recently-formed travertine precipitate	Calcite	None
OM10-2COPS-MG	Qafeefah Travertine	0646072	2533678	Recently-formed travertine precipitate	Aragonite	Brucite, calcite, unidentified clay
OM10-28C-MG-WHITE	Misht Travertine	0487358	2576102	Travertine terrace	Calcite	dolomite, unidentified clay
OM10-28C-MG-BROWN	Misht Travertine	0487358	2576102	Travertine terrace	Dolomite, calcite	Aragonite, unidentified clay
OM10-29C-MG	Misht Travertine	0487323	2576088	Travertine terrace	Calcite	Dolomite, unidentified clay
OM10-32C-MG-#1	Misht Travertine	0487305	2576134	Travertine terrace, part of sequence	Calcite	None
OM10-32C-MG-#2	Misht Travertine	0487305	2576134	Travertine terrace, part of sequence	Calcite	Smectite-kaolinite
OM10-32C-MG-#3	Misht Travertine	0487305	2576134	Travertine terrace, part of sequence	Calcite	Unidentified clay
OM10-32C-MG-#4	Misht Travertine	0487305	2576134	Travertine terrace, part of sequence	Calcite	Kaolinite, other unidentified clay
OM10-32C-MG-#5	Misht Travertine	0487305	2576134	Travertine terrace, part of sequence	Calcite	Kaolinite, other unidentified clay
OM10-32C-MG-#6	Misht Travertine	0487305	2576134	Travertine terrace, part of sequence	Calcite	Dolomite, kaolinite, other unidentified clay
OM10-32C-MG-#7	Misht Travertine	0487306	2576134	Travertine terrace, part of sequence	Calcite	Unidentified clay
OM10-32C-MG-#8	Misht Travertine	0487305	2576134	Travertine terrace, part of sequence	Calcite	None
OM10-32C-MG-#9	Misht Travertine	0487305	2576134	Travertine terrace, part of sequence	Calcite	None
OM10-32C-MG-#10	Misht Travertine	0487305	2576134	Travertine terrace, part of sequence	Calcite	Unidentified clay
OM10-32C-MG-#11	Misht Travertine	0487305	2576134	Travertine terrace, part of sequence	Calcite	Unidentified clay
OM10-31C-MG	Misht Travertine	0487305	2576134	Travertine terrace, part of sequence w/ 32C	Calcite	Unidentified clay
OM10-33C-MG	Misht Travertine	0487305	2576134	Travertine terrace, part of sequence w/ 32C	Calcite	Unidentified clay
OM10-36C-MG	Misht Travertine	0487322	2576050	Travertine terrace	Calcite	Unidentified clay
OM10-38C-MG	Misht Travertine	0487316	2576132	Travertine vein	Calcite	Brucite (small amount)
OM10-13P-MG	Misht Travertine	0487305	2576134	Travertine vein	Calcite	Hydromagnesite?, unidentified clay

Table 1. (*continued*)

Sample name	Location	UTM-Easting	UTM-Northing	Description	Major minerals (XRD)	Minor minerals (XRD)
OM10-37C-MG	Misht Travertine	0487322	2576050	Channel-filling travertine	Dolomite	Chrysotile, unidentified clay
OM10-39C-MG	Misht Travertine	0487316	2576132	Channel-filling travertine	Calcite	Unidentified clay
OM10-6COPS-MG	Misht Travertine	0487316	2576132	Recently-formed travertine precipitate	Calcite	Aragonite?, unidentified clay
OM09-88C-MS	Wadi Sudari Travertine	0443088	2650306	Terrace travertine	Calcite	Unidentified clay
OM09-76C-MS-A	Wadi Suadari Travertine	0443115	2650257	Speleothem-like, layered travertine (drop)	Calcite	None
OM09-76C-MS-B	Wadi Suadari Travertine	0443115	2650257	Speleothem-like, layered travertine (drop)	Calcite	Unidentified clay (very small amount)
OM09-76C-MS-C	Wadi Suadari Travertine	0443115	2650257	Speleothem-like, layered travertine (drop)	Calcite	Unidentified clay (very small amount)
OM09-85C-MS	Wadi Sudari Travertine	0443082	2650304	Newly-formed, stalagmite-like travertine	Calcite	Unidentified clay
OM09-84C-MS	Wadi Sudari Travertine	0443082	2650304	Travertine vein	Calcite, brucite	Hydromagnesite?, unidentified clay
OM09-87C-MS	Wadi Sudari Travertine	0443069	2650312	Travertine vein	Calcite	Dolomite
OM09-86C-MS	Wadi Sudari Travertine	0443069	2650312	Channel-filling travertine	Calcite	Dolomite, unidentified clay
OM09-81C-MS	Wadi Sudari Travertine	0443115	2650257	Channel-filling travertine	Calcite	Unidentified clay
OM09-89C-MS	Wadi Sudari Travertine	0443118	2650078	Channel-filling travertine	Calcite	Aragonite, brucite
OM09-8COPS-MS	Wadi Sudari Travertine	0443118	2650078	Recently-formed travertine precipitate	Calcite	Aragonite, hydromagnesite?, unidentified clay
OM09-106C-MS-A	Wadi Uqaybah Travertine	0426245	2633924	Terrace travertine	Calcite	None
OM09-106C-MS-B	Wadi Uqaybah Travertine	0426245	2633924	Terrace travertine	Calcite	Unidentified clay
OM10-78C-MG-#1	Wadi Uqaybah Travertine	0426266	2633919	Terrace travertine, part of sequence	Halite	Calcite, dolomite, unidentified clay
OM10-78C-MG-#2	Wadi Uqaybah Travertine	0426266	2633919	Terrace travertine, part of sequence	Halite	Dolomite, unidentified clay
OM10-78C-MG-#3	Wadi Uqaybah Travertine	0426266	2633919	Terrace travertine, part of sequence	Calcite	Unidentified clay
OM10-78C-MG-#4	Wadi Uqaybah Travertine	0426266	2633919	Terrace travertine, part of sequence	Calcite	Dolomite, unidentified clay
OM10-78C-MG-#5	Wadi Uqaybah Travertine	0426266	2633919	Terrace travertine, part of sequence	Calcite	Unidentified clay
OM10-78C-MG-#6	Wadi Uqaybah Travertine	0426266	2633919	Terrace travertine, part of sequence	Calcite	Unidentified clay
OM09-107C-MS	Wadi Uqaybah Travertine	0426309	2633950	Terrace travertine, part of sequence	Calcite	Unidentified clay
OM09-108C-MS	Wadi Uqaybah Travertine	0426215	2633925	Travertine vein	Dolomite	Monohydrocalcite?, quartz?
OM09-109C-MS	Wadi Uqaybah Travertine	0426208	2633925	Channel-filling travertine	Calcite	None
OM10-10COPS-MS	Wadi Uqaybah Travertine	0426183	2633965	Recently-formed travertine precipitate	Calcite	Quartz?, unidentified clay
Mg-rich carbonate outcrop veins						
OM09-47C-MS	Fanja Roadcut	0609304	2597565	Carbonate outcrop vein	Magnesite	Unidentified clay
OM10-13C-MG	Fanja Roadcut	0609451	2597416	Carbonate outcrop vein	Magnesite	Dolomite, calcite
OM10-53C-MG	Al-Wuqbah Roadcut	0440574	2643360	Carbonate outcrop vein	Magnesite	None
OM09-91C-MS	Wadi Sudari Campsite	0446151	2647471	Carbonate outcrop vein	Magnesite	Calcite

(*continued on next page*)

Table 1. (*continued*)

Sample name	Location	UTM-Easting	UTM-Northing	Description	Major minerals (XRD)	Minor minerals (XRD)
OM10-82C-MG	Wadi Sudari Campsite	0445905	2647602	Carbonate outcrop vein	Magnesite	Dolomite, calcite, unidentified clay
OM10-83C-MG	Wadi Sudari Campsite	0445905	2647602	Carbonate outcrop vein	Dolomite, calcite	Magnesite, unidentified clay
OM10-84C-MG	Wadi Sudari Campsite	0445991	2647684	Carbonate outcrop vein	Brucite, calcite	Magnesite, dolomite, unidentified clay
Mg-rich carbonate roadcut veins						
OM09-35C-MS	Qafeefah Roadcut	0647852	2537682	Carbonate/serpentine roadcut vein	Magnesite	Chrysotile, unidentified clay
OM09-36C-MS	Qafeefah Roadcut	0647818	2537657	Carbonate roadcut vein	Magnesite	Calcite, dolomite
OM09-37C-MS	Qafeefah Roadcut	0647821	2537649	Carbonate/serpentine roadcut vein	Dolomite	Magnesite, chrysotile, calcite, brucite, unidentified clay
OM10-24C-MG	Qafeefah Roadcut	0647791	2537644	Carbonate/serpentine roadcut vein	Magnesite	Chrysotile, dolomite
OM10-26C-MG	Qafeefah Roadcut	0647791	2537644	Carbonate/serpentine roadcut vein	Magnesite	Kaolinite, dolomite
OM10-27C-MG	Qafeefah Roadcut	0647791	2537644	Carbonate/serpentine roadcut vein	Magnesite	Kaolinite, dolomite
OM09-38C-MS	Qafeefah Roadcut	0647782	2537641	Thin carbonate on roadcut surface	Magnesite	Dolomite, unidentified clay
OM10-25C-MG	Qafeefah Roadcut	0647791	2537644	Thin carbonate on roadcut surface	Magnesite	Dolomite, halite
OM09-55C-MS	Fanja Roadcut	0609351	2597507	Carbonate/serpentine roadcut vein	Dolomite	Aragonite?, unidentified clay
OM09-57C-MS	Fanja Roadcut	0609356	2597501	Carbonate/serpentine roadcut vein	Dolomite	Aragonite?, calcite, unidentified clay
OM09-58C-MS	Fanja Roadcut	0609370	2597506	Carbonate/serpentine roadcut vein	Dolomite, periclase?	Aragonite?, unidentified clay
OM09-60C-MS	Fanja Roadcut	0609368	2597494	Carbonate/serpentine roadcut vein	Dolomite	Magnesite, kaolinite, other unidentified clay
OM09-61C-MS	Fanja Roadcut	0609379	2597499	Carbonate roadcut vein	Magnesite	Dolomite
OM09-62C-MS	Fanja Roadcut	0609470	2597481	Carbonate roadcut vein	Magnesite	None
OM09-63C-MS	Fanja Roadcut	0609470	2597481	Carbonate roadcut vein	Magnesite	Unidentified clay
OM09-64C-MS	Fanja Roadcut	0609470	2597481	Carbonate roadcut vein	Magnesite	Dolomite
OM09-50C-MS	Fanja Roadcut	0609279	2597526	Thin carbonate on roadcut surface	Dolomite, magnesite	Unidentified clay
OM10-48C-MG	Al-Wuqbah Roadcut	0440574	2643360	Carbonate/serpentine roadcut vein	Dolomite	Chrysotile, kaolinite, other unidentified clay
OM10-51C-MG	Al-Wuqbah Roadcut	0440396	2643047	Carbonate roadcut vein	Brucite, calcite, chrysotile	Dolomite, kaolinite, other unidentified clay
OM10-52C-MG	Al-Wuqbah Roadcut	0440396	2643047	Carbonate roadcut vein	Magnesite	Halite?, unidentified clay
OM10-54C-MG	Al-Wuqbah Roadcut	0440832	2643931	Carbonate/serpentine roadcut vein	Dolomite	Smectite-kaolinite, other unidentified clay
OM10-47C-MG-CLEAR	Al-Wuqbah Roadcut	0440574	2643360	Thin carbonate on roadcut surface	Dolomite	Aragonite?, unidentified clay
OM10-47C-MG-OPAQUE	Al-Wuqbah Roadcut	0440574	2643360	Thin carbonate on roadcut surface	Dolomite	Magnesite, calcite
OM10-49C-MG	Al-Wuqbah Roadcut	0440574	2643360	Thin carbonate on roadcut surface	Dolomite	Magnesite, unidentified clay

Initial ^{14}C dating was carried out using the standard acid dissolution method. Additional ^{14}C dating was carried out using a sealed tube graphitization method, which has a precision of 2 to 3‰ (Xu et al., 2007; Burke et al., 2010), similar to the precision typically obtained for samples analyzed by the standard dissolution method (Mark Roberts, personal communication, 2012).

The reproducibility of the ^{14}C measurements was evaluated through (1) duplicate standard acid dissolution analyses on ten samples and (2) triplicate sealed tube

Table 2
^{14}C data and ages.

Sample name	^{14}C dating technique	Fraction modern ^{14}C	Error	Uncalibrated ^{14}C age (yr BP)	Error	Calibrated ^{14}C age (yr BP)	Error
Travertines							
OM09-27C-MS	Standard hydrolysis	0.2797	0.0027	10,250	75	11,971	152
OM09-31C-MS	Standard hydrolysis	0.0968	0.0010	18,750	80	22,351	103
OM09-32C-MS-WHITE	Standard hydrolysis	0.0105	0.0006	36,600	450	42,299	337
OM09-32C-MS-BROWN	Standard hydrolysis	0.0484	0.0008	24,300	130	29,158	249
OM09-33C-MS	Standard hydrolysis	0.5868	0.0023	4280	30	4848	11
OM09-28C-MS	Standard hydrolysis	0.5661	0.0026	4570	35	3351	19
OM09-6COPS-MS	Standard hydrolysis	0.9710	0.0034	235	30	294	12
OM09-7COPS-MS	Sealed tube	0.9569	0.0052	354	44	350	30
OM10-1COPS-MG	Sealed tube	1.0064	0.0047	>modern	–	> modern	–
OM10-2COPS-MG	Sealed tube	*1.0017*	*0.0072*	>modern	–	>modern	–
		1.0026	*0.0054*	>modern	–	>modern	–
		1.0022	**0.0063**	**>modern**	–	**>modern**	–
OM10-28C-MG-WHITE	Sealed tube	0.0200	0.0012	31,406	483	35,685	359
OM10-28C-MG-BROWN	Sealed tube	0.4092	0.0026	7178	52	7987	41
OM10-29C-MG	Sealed tube	0.1601	0.0019	14,715	94	17,861	166
OM10-32C-MG-#1	Sealed tube	*0.0080*	*0.0012*	*38,325*	*1209*	*38,325*	*1209*
		0.0052	*0.0012*	*42,260*	*1830*	*43,183*	*877*
		0.0060	*0.0013*	*41,155*	*1714*	*45,748*	*1631*
		0.0064	**0.0012**	**40,580**	**1584**	**44,689**	**1326**
OM10-32C-MG-#2	Sealed tube	0.0088	0.0012	38,015	1073	42,544	1564
OM10-32C-MG-#3	Sealed tube	0.0065	0.0012	40,464	1457	40,464	1457
OM10-32C-MG-#4	Sealed tube	0.0076	0.0012	39,157	1237	43,393	885
OM10-32C-MG-#5	Sealed tube	0.0231	0.0013	30,277	443	34,887	381
OM10-32C-MG-#6	Sealed tube	0.0259	0.0012	29,347	385	34,044	476
OM10-32C-MG-#7	Sealed tube	–	–	–	–	–	–
OM10-32C-MG-#8	Sealed tube	0.1854	0.0022	13,535	96	16,710	133
OM10-32C-MG-#9	Sealed tube	0.0311	0.0013	27,867	324	32,012	448
OM10-32C-MG-#10	Sealed tube	0.0843	0.0016	19,866	153	23,708	215
OM10-32C-MG-#11	Sealed tube	0.3689	0.0022	8011	48	8891	31
OM10-31C-MG	Sealed tube	0.0490	0.0013	24,231	221	29,051	148
OM10-33C-MG	Sealed tube	0.0329	0.0013	27,425	306	31,564	277
OM10-36C-MG	Sealed tube	0.0378	0.0013	26,317	277	30,971	201
OM10-38C-MG	Sealed tube	0.2329	0.0020	11,705	69	13,547	102
OM10-13P-MG	Sealed tube	0.0838	0.0015	19,915	141	23,750	221
OM10-37C-MG	Sealed tube	0.7644	0.0042	2159	45	2144	36
OM10-39C-MG	Sealed tube	0.7227	0.0047	2609	53	2746	40
OM10-6COPS-MG	Sealed tube	1.0036	0.0052	>modern	–	>modern	–
OM09-88C-MS	Standard hydrolysis	*0.0200*	*0.0005*	*31,400*	*180*	*35,692*	*266*
		0.0302	*0.0007*	*28,100*	*200*	*32,297*	*392*
		0.0251	**0.0006**	**29,750**	**190**	**33,995**	**329**
OM09-76C-MS-A	Standard hydrolysis	0.0254	0.0005	29,500	160	34,289	302
OM09-76C-MS-B	Standard hydrolysis	0.0140	0.0004	34,300	230	39,166	352
OM09-76C-MS-C	Standard hydrolysis	0.0075	0.0003	39,300	320	43,455	336
OM09-85C-MS	Standard hydrolysis	*1.5496*	*0.0048*	*>modern*	–	*>modern*	–
		1.4632	*0.0064*	*>modern*	–	*>modern*	–
		1.5064	**0.0056**	**>modern**	**–**	**>modern**	**–**
OM09-84C-MS	Standard hydrolysis	*0.1294*	*0.0014*	*16,450*	*90*	*19,512*	*145*
		0.1513	*0.0014*	*15,150*	*70*	*18,200*	*175*
		0.1403	**0.0014**	**15,800**	**80**	**18,856**	**160**
OM09-87C-MS	Standard hydrolysis	0.0824	0.0008	20,100	80	24,032	165
OM09-86C-MS	Standard hydrolysis	*0.4601*	*0.0019*	*6240*	*35*	*7204*	*48*
		0.3759	*0.0021*	*7860*	*45*	*8655*	*65*
		0.4180	**0.0020**	**7050**	**40**	**7929**	**56**
OM09-81C-MS	Standard hydrolysis	1.043	0.0036	>modern	–	>modern	–
OM09-89C-MS	Standard hydrolysis	1.003	0.0042	>modern	–	>modern	–
OM09-8COPS-MS	Standard hydrolysis	1.014	0.0031	>modern	–	>modern	–
OM09-106C-MS-A	Standard hydrolysis	0.0433	0.0007	25,200	130	30,023	235
OM09-106C-MS-B	Standard hydrolysis	*0.0212*	*0.0006*	*31,000*	*230*	*35,316*	*232*
		0.0290	*0.0007*	*28,400*	*190*	*32,772*	*366*
		0.0251	**0.0007**	**29,700**	**210**	**34,044**	**299**

(*continued on next page*)

Table 2. (*continued*)

Sample name	^{14}C dating technique	Fraction modern ^{14}C	Error	Uncalibrated ^{14}C age (yr BP)	Error	Calibrated ^{14}C age (yr BP)	Error
OM10-78C-MG-#1	–	–	–	–	–	–	–
OM10-78C-MG-#2	–	–	–	–	–	–	–
OM10-78C-MG-#3	Sealed tube	*0.0114*	*0.0012*	*35,920*	*841*	*41,005*	*816*
		0.0102	*0.0012*	*36,829*	*939*	*41,745*	*731*
		0.0096	*0.0013*	*37,322*	*1067*	*42,074*	*793*
		0.0104	**0.0012**	**36,690**	**949**	**41,608**	**780**
OM10-78C-MG-#4	Sealed tube	0.0138	0.0012	34,427	688	39,532	831
OM10-78C-MG-#5	Sealed tube	0.0089	0.0012	37,949	1062	42,499	772
OM10-78C-MG-#6	Sealed tube	0.0170	0.0019	32,727	894	37,544	995
OM09-107C-MS	Standard hydrolysis	0.0270	0.0005	29,000	150	33,599	358
OM09-108C-MS	Standard hydrolysis	0.3659	0.0020	8070	45	9005	29
OM09-109C-MS	Standard hydrolysis	*0.5326*	*0.0026*	*5060*	*40*	*5867*	*25*
		0.5536	*0.0024*	*4750*	*35*	*5543*	*78*
		0.5431	**0.0025**	**4905**	**38**	**5705**	**52**
OM09-10COPS-MS	Standard hydrolysis	1.005	0.0035	>modern	–	>modern	–
Mg-rich carbonate outcrop veins							
OM09-47C-MS	Standard hydrolysis	*0.0517*	*0.0009*	*23,800*	*140*	*28,559*	*239*
		0.0510	*0.0006*	*23,900*	*90*	*28,660*	*210*
		0.0514	**0.0008**	**23,850**	**115**	**28,610**	**225**
OM10-13C-MG	Sealed tube	0.0093	0.0012	37,534	1012	42,220	731
OM10-53C-MG	Sealed tube	*0.0091*	*0.0012*	*37,783*	*1036*	*42,387*	*747*
		0.0072	*0.0012*	*39,628*	*1336*	*43,688*	*948*
		0.0079	*0.0012*	*38,918*	*1207*	*43,246*	*873*
		0.0080	**0.0012**	**38,776**	**1193**	**43,107**	**856**
OM09-91C-MS	Standard hydrolysis	0.0254	0.0006	29,500	180	34,277	320
OM10-82C-MG	Sealed tube	0.0158	0.0013	33,318	639	37,960	780
OM10-83C-MG	Sealed tube	0.0085	0.0012	38,333	1124	42,782	830
OM10-84C-MG	Sealed tube	0.0261	0.0012	29,281	374	34,007	481
Mg-rich carbonate roadcut veins							
OM09-35C-MS	Sealed tube	0.0057	0.0012	41,547	1684	48,496	1366
OM09-36C-MS	Sealed tube	−0.0008	0.0012	>50,000	–	>50,000	–
OM09-37C-MS	Sealed tube	0.0036	0.0012	45,275	2623	>50,000	–
OM10-24C-MG	Sealed tube	0.0432	0.0015	25,240	279	30,007	312
OM10-26C-MG	Sealed tube	0.0995	0.0015	18,535	118	22,179	199
OM10-27C-MG	Sealed tube	0.0452	0.0017	24,879	302	29,697	202
OM09-38C-MS	Sealed tube	0.0181	0.0012	32,214	552	38,450	649
OM10-25C-MG	Sealed tube	0.0567	0.0014	23,057	205	27,922	286
OM09-55C-MS	Standard hydrolysis	*0.0008*	*0.0002*	*>50,000*	–	*>50,000*	–
		0.0004	*0.0002*	*>50,000*	–	*>50,000*	–
		0.0006	**0.0002**	**>50,000**	**–**	**>50,000**	**–**
OM09-57C-MS	Standard hydrolysis	*0.0010*	*0.0002*	*>50,000*	–	*>50,000*	–
		0.0007	*0.0002*	*>50,000*	–	*>50,000*	–
		0.0009	**0.0002**	**>50,000**	**–**	**>50,000**	**–**
OM09-58C-MS	Standard hydrolysis	0.0015	0.0004	>50,000	–	>50,000	–
OM09-60C-MS	Standard hydrolysis	0.0015	0.0002	>50,000	–	>50,000	–
OM09-61C-MS	Standard hydrolysis	0.0032	0.0003	46,100	660	>50,000	–
OM09-62C-MS	Standard hydrolysis	0.0016	0.0005	>50,000	–	>50,000	–
OM09-63C-MS	Standard hydrolysis	0.0030	0.0003	46,600	860	>50,000	–
OM09-64C-MS	Standard hydrolysis	0.0045	0.0004	43,500	660	44,497	651
OM09-50C-MS	Standard hydrolysis	*0.0364*	*0.0005*	*26,600*	*120*	*31,139*	*82*
		0.0353	*0.0006*	*26,900*	*150*	*31,256*	*93*
		0.0358	**0.0006**	**26,750**	**135**	**31,197**	**87**
OM10-48C-MG	Sealed tube	0.0007	0.0012	>50,000	–	>50,000	–
OM10-51C-MG	Sealed tube	0.0805	0.0015	20,240	150	24,154	201
OM10-52C-MG	Sealed tube	0.0097	0.0012	37,238	1013	43,644	749
OM10-54C-MG	Sealed tube	0.0092	0.0012	37,623	1076	42,278	785
OM10-47C-MG-CLEAR	Sealed tube	0.0011	0.0012	>50,000	–	>50,000	–
OM10-47C-MG-OPAQUE	Sealed tube	0.0293	0.0012	28,365	341	32,643	525
OM10-49C-MG	Sealed tube	*0.0215*	*0.0012*	*30,855*	*459*	*35,234*	*347*
		0.0156	*0.0012*	*33,420*	*611*	*38,054*	*772*
		0.0149	*0.0013*	*33,799*	*716*	*38,497*	*1010*
		0.0173	**0.0012**	**32,691**	**595**	**37,261**	**709**

Replicate analyses are indicated in italics, with the average of replicate analyses given in bold.

graphitization analyses on five samples (see Table 2). The reproducibility of Fraction Modern[2] (F_m) ^{14}C ranges from <1 to 9%, with an average of 2%, for the standard acid dissolution method. The reproducibility is the worst for a younger sample (OM09-85C-MS) with very high F_m and also for layered travertine samples OM09-86C-MG and OM09-106C-MS-B, which may not have been subsampled on a sufficiently fine scale. The variability of replicate ^{14}C analyses on layered travertines results in calibrated age differences of up to 2000 to 3000 years. The reproducibility of F_m for the sealed tube graphitization method is 1 to 3%. The better reproducibility of the sealed tube graphitization analyses may reflect improvements in carbonate subsampling that were made after the first batch of travertine ^{14}C analyses.

Two samples were analyzed by both the standard acid dissolution and the sealed tube graphitization methods to check the agreement of the methods. Sample OM09-109C-MS, a channel-filling travertine, produced calibrated ^{14}C ages of 5867 ± 25 yr BP and 5543 ± 78 yr BP (average: 5705 yr BP) via the standard acid dissolution method and 5773 ± 129 yr BP via the sealed tube graphitization method. Sample OM09-47C-MS, a carbonate outcrop vein, produced calibrated ^{14}C ages of 28,559 ± 239 yr BP and 28,660 ± 210 yr BP (average: 28,610 yr BP) via the standard acid dissolution method and 30,526 ± 263 yr BP via the sealed tube graphitization method. Therefore, the standard acid dissolution and sealed tube graphitization methods agree reasonably well.

For the standard acid dissolution method, the CO_2 gas was then combined with H_2 gas and heated in the presence of an iron catalyst to make graphite (Vogel et al., 1987). This graphite was then pressed into targets, which were analyzed for $^{14}C/^{12}C$ ratios on a 2.5 MV tandetron accelerator mass spectrometer (AMS-1). For the sealed tube graphitization method, the CO_2 was converted to graphite using a zinc reduction method (Xu et al., 2007; Burke et al., 2010). This graphite was stored in the sealed reaction tubes until immediately prior to pressing the graphite into targets. These targets were analyzed on a 500 kV compact pelletron accelerator (CFAMS; Roberts et al., 2009).

For both the standard acid dissolution and sealed tube graphitization methods, primary and secondary standards and blanks were routinely measured. Secondary standards were analyzed with every 8–10 samples. The primary standard was NBS Oxalic Acid I (NIST-SRM-4990, $F_m = 1.0397$), and the secondary standards were IAEA C-2 ($F_m = 0.4114$; Rozanski et al., 1992), TIRI-I ($F_m = 0.2524$; Scott, 2003), and FIRI-C ($F_m = 0.1041$; Boaretto et al., 2002). Blank corrections were made using analyses of the ^{14}C dead IAEA C-1 Carrara marble and Alfa Aeasar graphite (for the AMS machine background). Blanks for IAEA C-1 are $F_m = 0.0017 \pm 0.009$ for the standard acid dissolution (equivalent to a ^{14}C age of 51,227 yr BP; $n = 112$; routine measurements by NOSAMS staff) and $F_m = 0.0023 \pm 0.0006$ (equivalent to a ^{14}C age of 48,664 yr BP; $n = 7$) for the sealed tube graphitization method.

Results of the ^{14}C analyses are reported as Fraction Modern (F_m) and as both uncalibrated and calibrated ^{14}C ages in yr BP (Before Present where Present = A.D. 1950 by convention). The F_m results were calculated using the internationally accepted modern value of 1.176×10^{-12} (Karlen et al., 1964). The sample F_m was also corrected to a $\delta^{13}C$ VPDB value of −25‰. The uncalibrated ^{14}C ages were calculated from F_m using 5568 years as the half-life of radiocarbon and following the convention in Stuiver and Polach (1977) and Stuiver (1980). Calibrated ^{14}C ages were obtained using the Calib 6.0 Program with the IntCal09 calibration curve (Reimer et al., 2009).

C and O isotopic analyses were conducted at the University of Michigan Stable Isotope Laboratory using a Finnigan MAT Kiel IV preparation device coupled directly to the inlet of a Finnigan MAT 253 triple collector isotope ratio mass spectrometer (see methods in Ivany et al., 2008). Measured precision was maintained at better than 0.1‰ for both C and O isotope compositions.

5. RESULTS

5.1. Mineralogy

The minerals identified through analysis of XRD data are presented in Table 1. Mineral peaks were identified as "major" or "minor" but were not further quantified. The travertine terraces, travertine veins, and pseudospeleothems have fairly uniform mineral compositions and are composed of almost pure calcite with minor amounts of other minerals such as serpentine, clay, and dolomite (common) as well as aragonite, brucite, and hydromagnesite (less common). The recently formed travertine precipitates consist predominantly of either calcite or aragonite. The majority of the Mg-rich carbonate veins consist predominantly of magnesite with minor clay and sometimes minor dolomite, calcite, and serpentine. A few of the Mg-rich carbonate veins, primarily those sampled at roadcuts, consist predominantly of dolomite rather than magnesite. This may be because dolomite, which is more soluble than magnesite, is better preserved at roadcuts, where the carbonate veins are generally less weathered.

5.2. Distribution of carbonate ^{14}C ages

Results of the ^{14}C analyses are reported as F_m and as both uncalibrated and calibrated ^{14}C ages in yr BP in Table 1. Replicate analyses (done in 2009) for two Kelemen and Matter (2008) samples (OM07–07 and OM07–57) are also presented in Table 2.

5.2.1. Travertines

The distribution of calibrated ^{14}C ages for surface travertines and Ca-rich travertine veins is presented in Figs. 6 and 7 and in Supplementary Figure S1. Note that in all Figures presenting ^{14}C ages we have used a cut-off of 45,000 years to facilitate comparisons with the earlier data

---

[2] Fraction Modern (F_m) ^{14}C is defined as the deviation of a sample from "modern", where modern is defined as 95% of the radioactive carbon concentration (in A.D. 1950) of NBS Oxalic Acid I normalized to $\delta^{13}C$ VPDB = −19‰ (Olsson, 1970).

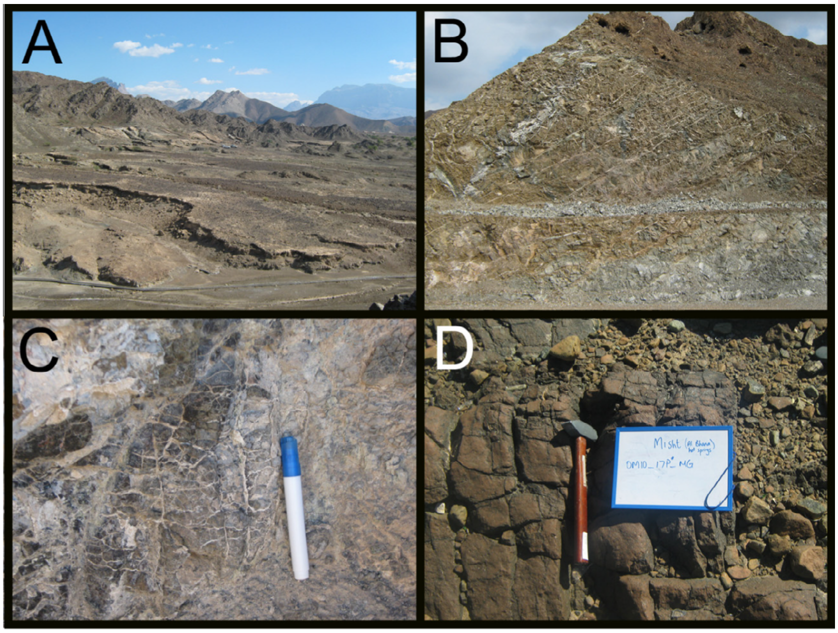

Fig. 5. Representative images of altered peridotites in the Samail Ophiolite. A: Small hills of altered peridotite are visible (background) adjacent to travertine terraces at Misht Travertine. B: Highly-altered peridotite with abundant carbonate-serpentine veins at Fanja Roadcut. Note how the natural peridotite weathering surface is visible above the roadcut. The roadcut is ~5 m in height. C: Very highly altered peridotite exposed underneath a travertine terrace at Misht Travertine. Note the marker for scale. D: Highly-altered peridotite exposed at Misht Travertine. Note the hammer for scale.

of Clark and Fontes (1990). Surface travertine deposits from this and other studies (Clark and Fontes, 1990; Clark et al., 1992; Kelemen and Matter, 2008; Kelemen et al., 2011) range in age from modern to >45,000 yr BP, indicating long-term deposition and preservation.

A number of the samples, including recently-formed travertines, channel-filling travertines, and the actively-forming pseudospeleothem, have $F_m > 1.00$ (Table 2). Clark et al. (1992), Kelemen and Matter (2008), and Kelemen et al. (2011) also observed travertines with $F_m > 1.00$. Travertines with $F_m > 1.00$ were deposited after A.D. 1950 and contain C that is primarily atmospheric in origin. However, some samples with F_m values lower than the current values in the Northern Hemisphere troposphere provide evidence for incorporation of a small amount of older, non-atmospheric C, which may be recycled from older travertines or carbonate veins that are being weathered. Samples from travertine terraces ($n = 28$) range in age from ~8000 to 45,000 yr BP with an average age of ~31,000 yr BP. However, it is important to note that there are some sampling biases in the travertine terrace dataset. Most of the samples were collected from the tops of travertine terraces. Additionally, three travertine terraces were subsampled (see Supplementary Figures S2 to S4). For example, 12 (out of 16) of the travertine terrace samples from Misht Travertine were collected from the same ~2 m thick terrace exposure. The oldest travertine in the Misht terrace sequence (~45,000 yr BP) is found at the bottom of the terrace, just above the altered peridotite bedrock. The upper layer of the Misht terrace sequence has an age of ~29,000 yr BP. At Wadi Uqaybah Travertine, two ~1 m thick terraces were subsampled. The first terrace ranges in age from ~38,000 to 42,000 yr BP (4 subsamples) with one sample having an anomalously old age compared to the samples above and below it. The second terrace ranges in age from ~30,000 to 34,000 yr BP (2 subsamples).

Ca-rich veins associated with travertine deposits are generally younger than the Mg-rich veins sampled at roadcuts and outcrops far from travertines. The travertine vein samples ($n = 5$) have ages ranging from ~5000 to 24,000 yr BP with an average age of ~14,000 yr BP. This range of ages is similar to the range previously obtained by Clark and Fontes (1990), who obtained ages of ~6500 to 36,000 yr BP (average: ~16,000 yr BP), and by Kelemen and co-workers (Kelemen and Matter, 2008; Kelemen et al., 2011), who obtained ages of ~7000 to 35,000 yr BP (average: ~18,000 yr BP).

5.2.2. *Mg-rich carbonate veins*

The distribution of calibrated ^{14}C ages for Mg-rich carbonate outcrop and roadcut veins is presented in Fig. 8 and in Supplementary Figure S5. Mg-rich carbonate outcrop veins ($n = 7$) from this study range in age from ~29,000 to 43,000 yr BP with an average age of ~38,000 yr BP. These ages are at the older end of the age range for outcrop veins of ~8000 to 45,000 yr BP (average: ~34,000 yr BP; $n = 21$) previously obtained by Kelemen and Matter (2008) and Kelemen et al. (2011). One outcrop vein analyzed by Kelemen and Matter (2008) was ^{14}C dead.

Mg-rich roadcut veins ($n = 24$) show a significantly different range of ages. While half of the roadcut veins range in age from ~22,000 to 45,000 yr BP with an average age of

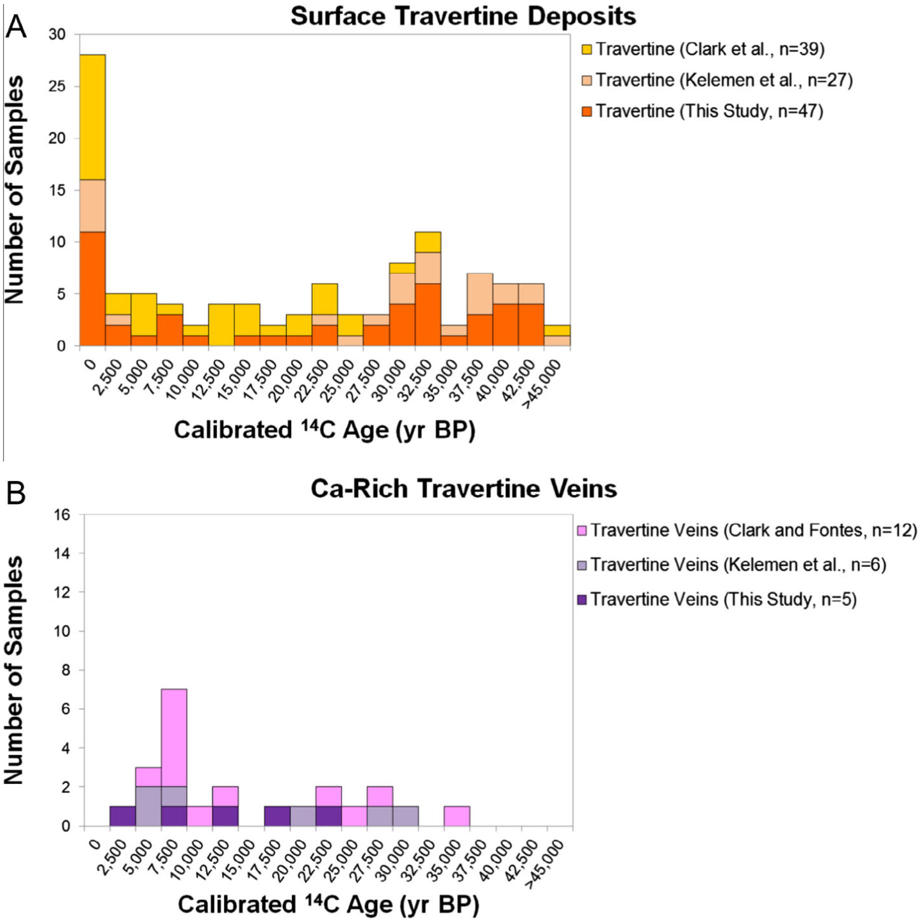

Fig. 6. Distribution of ^{14}C ages for travertines from the Samail Ophiolite. A: Distribution of ^{14}C ages for surface travertines. Data are from this study (dark orange bars); Kelemen and Matter (2008) and Kelemen et al. (2011) (light orange bars); and Clark and Fontes (1990) and Clark et al. (1992) (yellow bars). B: Distribution of ^{14}C ages for Ca-rich travertine veins. Data are from this study (dark purple bars); Kelemen and Matter (2008) and Kelemen et al. (2011) (light purple bars); and Clark and Fontes (1990) and Clark et al. (1992) (pink bars). Note that the ^{14}C data from this study and from Kelemen et al. were converted to calibrated ages using the method described in the text. Data from Clark et al. were calibrated using an older version of the ^{14}C calibration curve. Recalibration is not possible due to the unavailability of the uncalibrated data. (For interpretation of the references to color in this figure legend, the reader is referred to the web version of this article.)

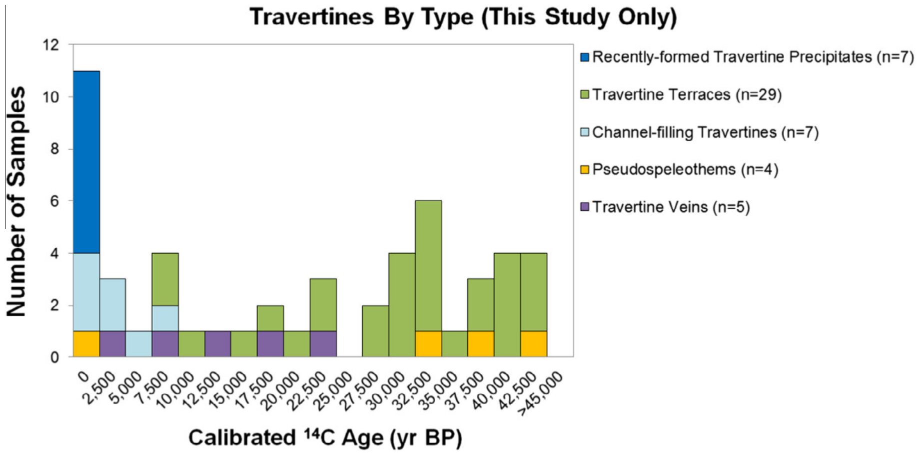

Fig. 7. Distribution of ^{14}C ages for different types of travertine from the Samail Ophiolite.

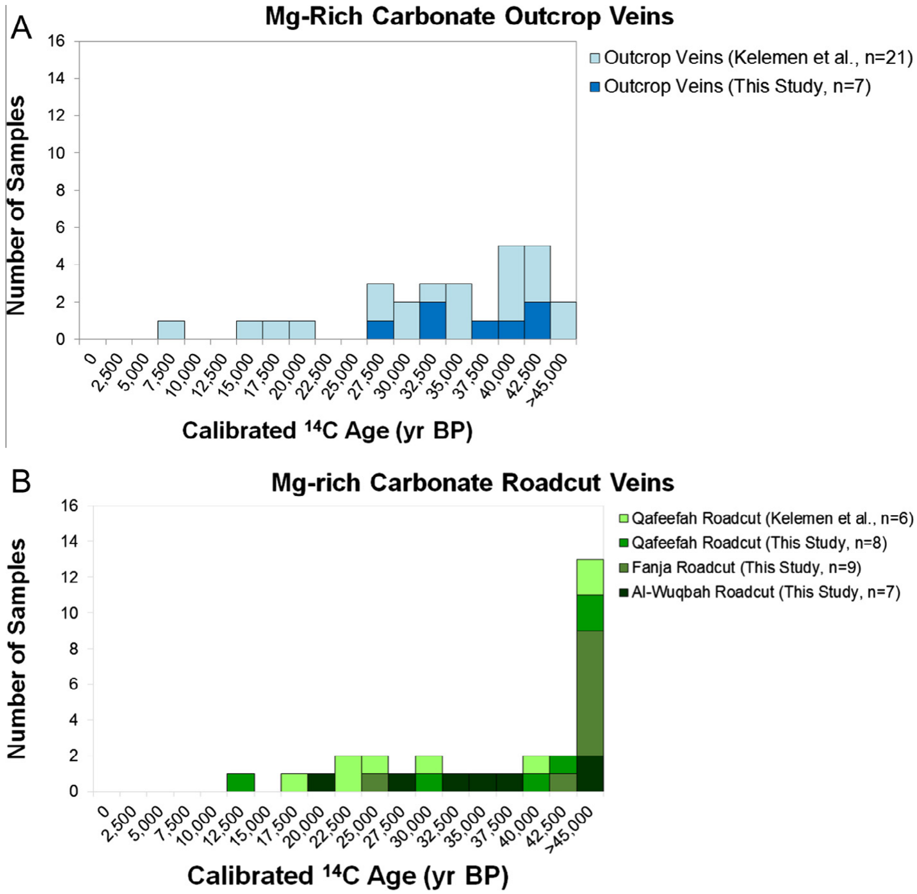

Fig. 8. Distribution of ^{14}C ages for Mg-rich carbonate veins from the Samail Ophiolite. A: ^{14}C ages for Mg-rich carbonate outcrop veins sampled on the natural peridotite weathering surface. Data are from this study (dark blue); Kelemen and Matter (2008) and Kelemen et al. (2011) (light blue). B: ^{14}C ages for Mg-rich carbonate roadcut veins. Data are from this study (darker greens); Kelemen and Matter (2008) and Kelemen et al. (2011) (light green). (For interpretation of the references to color in this figure legend, the reader is referred to the web version of this article.)

~34,000 yr BP (similar to the outcrop veins), the other half are ^{14}C dead. The majority of these were sampled from Fanja Roadcut, where 7 out of 9 individual veins are ^{14}C dead, and one other vein has an age of 44,497 ± 651 yr BP. At Qafeefah Roadcut, 3 out of 8 individual veins are ^{14}C dead. At Al-Wuqbah Roadcut, 2 out of 5 individual veins are ^{14}C dead. One of the two ^{14}C dead samples from Al-Wuqbah Roadcut comes from a heterogeneous vein that was subsampled into an opaque, chalky dolomite fraction (facing the roadcut's outer surface) and a clear, hard dolomite fraction (underneath). The opaque layer has an age of ~33,000 yr BP while the clear layer is ^{14}C dead. Two possible explanations for the age differences in this heterogeneous vein are: (1) the outer, opaque layer represents a part of the vein which has been affected by dissolution/re-precipitation, or (2) the outer, opaque layer represents a part of the vein which grew at a later time, thus indicating that veins can form over long time periods and/or were reactivated.

5.3. Stable isotope analyses

The results of δ^{13}C and δ^{18}O analyses of Samail carbonates are presented in Table 3 and plotted in Fig. 9. The δ^{13}C values are reported relative to the VPDB standard and the δ^{18}O values are reported relative to the VSMOW standard. Samail carbonates cover a wide range of C and O isotope compositions, ranging from approximately −27 to 5‰ for δ^{13}C and approximately 13 to 40‰ for δ^{18}O. The Mg-rich carbonate veins generally have higher isotopic ratios (average δ^{13}C: −5.22‰ ± 3.02‰ (1σ); average δ^{18}O: 32.46‰ ± 3.71‰ (1σ)) than the surface travertines (average δ^{13}C: −13.96‰ ± 7.27‰ (1σ); average δ^{18}O: 22.80‰ ± 5.06‰ (1σ)). This may in part be due to differences in mineralogy resulting in greater fractionation of the stable isotopes in Mg-carbonates than in Ca-carbonates. There is no significant difference between the isotopic compositions of Mg-rich carbonate outcrop veins (average δ^{13}C: −3.54‰ ± 2.73‰ (1σ); average δ^{18}O: 33.27‰ ± 4.24‰ (1σ)) versus roadcut veins (average δ^{13}C: −6.53‰ ± 2.40‰ (1σ); average δ^{18}O: 31.83‰ ± 3.10‰ (1σ)).

The travertines have roughly correlated δ^{13}C and δ^{18}O, which extend down to low ratios that are unusual for inorganic carbonates (see the extensive discussion on this in Kelemen et al., 2011). The travertine veins also tend to have higher stable isotope ratios (average δ^{13}C: −5.06‰ ± 4.84‰ (1σ); average δ^{18}O: 30.20‰ ± 4.27‰ (1σ)) than the surface travertines. A few of the surface

Table 3
Stable C and O isotope data.

Sample name	δ^{13}C VPDB	δ^{18}O VPDB	δ^{18}O VSMOW	δ^{18}O equilibrium temp. (°C)
Travertines				
OM09-27C-MS	*−5.63*	*−1.39*	*29.43*	
	−5.41	*−1.49*	*29.32*	
	−5.52	**−1.44**	**29.37**	11–19
OM09-31C-MS	−6.12	−2.88	27.89	17–26
OM09-32C-MS-WHITE	*−3.05*	*−4.99*	*25.72*	
	−3.04	*−4.92*	*25.79*	
	−3.04	**−4.95**	**25.75**	26–36
OM09-32C-MS-BROWN	−2.61	−0.63	30.21	–
OM09-33C-MS	2.78	6.36	37.42	−6 to −10
OM09-28C-MS	*−10.98*	*−6.54*	*24.12*	
	−10.89	*−6.39*	*24.27*	
	−10.93	**−6.47**	**24.19**	34–45
OM09-6COPS-MS	−15.96	−2.96	27.81	–
OM09-7COPS-MS	−18.62	−6.88	23.77	–
OM10-1COPS-MG	*−26.31*	*−16.27*	*14.09*	
	−26.30	*−16.33*	*14.03*	
	−26.31	**−16.30**	**14.06**	103–123
OM10-2COPS-MG	*−12.63*	*0.05*	*30.91*	
	−12.64	*0.07*	*30.93*	
	−12.64	**0.06**	**30.92**	–
OM10-28C-MG-WHITE	*−10.49*	*−2.93*	*27.84*	
	−10.66	*−2.99*	*27.78*	
	−10.58	**−2.96**	**27.81**	17–26
OM10-28C-MG-BROWN	1.34	3.48	34.45	–
OM10-29C-MG	−9.09	−4.65	26.07	25–35
OM10-32C-MG-#1	*−17.88*	*−7.79*	*22.83*	
	−17.77	*−7.64*	*22.98*	
	−17.82	**−7.71**	**22.91**	40–52
OM10-32C-MG-#2	*−14.84*	*−6.39*	*24.27*	
	−14.80	*−6.42*	*24.24*	
	−14.82	**−6.41**	**24.25**	33–44
OM10-32C-MG-#3	*−13.53*	*−11.53*	*18.98*	
	−13.57	*−11.50*	*19.01*	
	−13.66	*−11.52*	*18.99*	
	−13.58	**−11.51**	**18.99**	64–78
OM10-32C-MG-#4	*−18.19*	*−10.19*	*20.35*	
	−18.15	*−10.24*	*20.30*	
	−18.17	**−10.22**	**20.33**	55–69
OM10-32C-MG-#5	*−18.12*	*−10.43*	*20.11*	
	−18.08	*−10.49*	*20.05*	
	−18.10	**−10.46**	**20.08**	57–70
OM10-32C-MG-#6	*−20.56*	*−10.47*	*20.06*	
	−20.58	*−10.37*	*20.17*	
	−20.57	**−10.42**	**20.12**	56–70
OM10-32C-MG-#7	−17.13	−9.29	*21.28*	
	−17.38	−9.26	*21.32*	
	−17.17	−9.11	*21.47*	
	−17.23	**−9.22**	**21.36**	56–60
OM10-32C-MG-#8	*−17.04*	*−9.50*	*21.07*	
	−17.05	*−9.51*	*21.05*	
	−17.05	**−9.50**	**21.06**	51–64
OM10-32C-MG-#9	*−18.19*	*−10.26*	*20.28*	
	−18.03	*−10.30*	*20.24*	
	−18.11	**−10.28**	**20.26**	56–69
OM10-32C-MG-#10	*−11.21*	*−3.77*	*26.97*	
	−11.16	*−3.80*	*26.94*	
	−11.19	**−3.79**	**26.95**	21–30
OM10-32C-MG-#11	*−3.93*	*0.84*	*31.72*	
	−3.82	*0.74*	*31.62*	
	−3.87	**0.79**	**31.67**	2–10

(*continued on next page*)

Table 3. (*continued*)

Sample name	δ^{13}C VPDB	δ^{18}O VPDB	δ^{18}O VSMOW	δ^{18}O equilibrium temp. (°C)
OM10-31C-MG	*−10.72*	*−5.38*	*25.31*	
	−10.79	*−4.91*	*25.80*	
	−10.75	**−5.14**	**25.56**	27–37
OM10-33C-MG	−8.22	−3.78	26.96	21–30
OM10-36C-MG	−7.88	−8.04	22.57	42–54
OM10-38C-MG	*−7.99*	*1.04*	*31.93*	
	−8.04	*0.97*	*31.86*	
	−8.04	*1.14*	*32.03*	
	−8.02	**1.05**	**31.94**	1–9
OM10-13P-MG	−11.00	−4.79	25.92	25–35
OM10-37C-MG	0.20	1.78	32.69	21–30
OM10-39C-MG	−10.12	-5.80	24.88	30–41
OM10-6COPS-MG	*−22.98*	*−13.57*	*16.87*	
	-22.88	*−13.64*	*16.80*	
	−22.93	**−13.60**	**16.84**	79–96
OM09-88C-MS	−0.91	−8.93	21.65	47–60
OM09-76C-MS-A	*−14.21*	*−12.06*	*18.42*	
	−14.37	*−12.10*	*18.38*	
	−14.29	**−12.08**	**18.40**	68–83
OM09-76C-MS-B	−17.83	−15.88	14.49	99–118
OM09-76C-MS-C	−18.90	−16.07	14.29	100–120
OM09-85C-MS	−24.90	−14.26	16.16	84–102
OM09-84C-MS	−2.69	−5.47	25.22	–
OM09-87C-MS	*−8.76*	*−4.91*	*25.80*	
	−8.73	*−5.07*	*25.64*	
	−8.75	**−4.99**	**25.72**	26–36
OM09-86C-MS	−8.61	−9.72	20.84	52–65
OM09-81C-MS	−26.66	−15.73	14.64	97–117
OM09-89C-MS	−22.23	−12.52	17.95	71–86
OM09-8COPS-MS	−20.04	−8.74	21.85	46–58
OM09-106C-MS-A	−10.44	−4.97	25.74	23–33
OM09-106C-MS-B	−14.14	−8.87	21.72	47–59
OM10-78C-MG-#1	–	–	–	–
OM10-78C-MG-#2	–	–	–	–
OM10-78C-MG-#3	*−18.91*	*−11.36*	*19.15*	
	−18.93	*−11.38*	*19.13*	
	−18.92	**−11.37**	**19.14**	63–77
OM10-78C-MG-#4	*−20.24*	*−13.02*	*17.44*	
	−20.38	*−13.13*	*17.33*	
	−20.31	**−13.07**	**17.38**	75–91
OM10-78C-MG-#5	*−19.24*	*−11.04*	*19.48*	
	−19.14	*−10.93*	*19.60*	
	−19.19	**−10.98**	**19.54**	60–74
OM10-78C-MG-#6	*−5.16*	*−3.69*	*27.06*	
	−5.06	*-3.54*	*27.22*	
	−5.11	**−3.61**	**27.14**	20–29
OM09-107C-MS	−12.03	−6.42	24.24	33–44
OM09-108C-MS	*−2.81*	*−0.30*	*30.55*	
	−2.83	*−0.43*	*30.42*	
	−2.82	**−0.36**	**30.49**	21–35
OM09-109C-MS	*−11.17*	*−4.57*	*26.14*	
	−11.13	*−4.45*	*26.27*	
	−11.15	**−4.51**	**26.21**	24–34
OM09-10COPS-MS	−23.23	−14.60	15.81	87–105
Mg-rich carbonate outcrop veins				
OM09-47C-MS	−3.81	4.69	35.70	41–49
OM10-13C-MG	*−2.25*	*3.36*	34.33	
	−2.38	*3.47*	34.44	
	−2.31	**3.42**	**34.38**	46–55
OM10-53C-MG	*−0.79*	*3.58*	*34.55*	
	−0.69	*3.77*	*34.74*	
	−0.74	**3.67**	**34.64**	45–54

Table 3. (*continued*)

Sample name	δ^{13}C VPDB	δ^{18}O VPDB	δ^{18}O VSMOW	δ^{18}O equilibrium temp. (°C)
OM09-91C-MS	−3.45	2.44	33.37	50–60
OM10-82C-MG	*−5.95*	*2.49*	*33.42*	
	−5.99	*2.68*	*33.62*	
	−5.97	**2.58**	**33.52**	50–59
OM10-83C-MG	−10.41	−3.72	27.03	–
OM10–84C-MG	*−2.49*	*5.34*	*36.37*	
	−2.28	*5.24*	*36.26*	
	−2.38	**5.29**	**36.32**	–
Mg-rich carbonate roadcut veins				
OM09-35C-MS	*−7.19*	*2.64*	*33.58*	
	−7.07	*2.60*	*33.54*	
	−7.13	**2.62**	**33.56**	50–59
OM09-36C-MS	−6.32	0.82	31.70	58–68
OM09-37C-MS	−2.84	−0.50	30.34	52–62
OM10-24C-MG	*−6.42*	*2.04*	*32.96*	
	−6.39	*2.09*	*33.01*	
	−6.41	**2.06**	**32.99**	52–62
OM10-26C-MG	*−7.29*	*1.96*	*32.88*	
	−7.48	*2.02*	*32.94*	
	−7.38	**1.99**	**32.91**	53–62
OM10-27C-MG	*−7.05*	*2.35*	*33.29*	
	−7.09	*2.28*	*33.21*	
	−7.07	**2.32**	**33.25**	51–61
OM09-38C-MS	*−7.99*	*1.04*	*31.93*	
	−8.04	*0.97*	*31.86*	
	−8.04	*1.14*	*32.03*	
	−8.02	**1.05**	**31.94**	57–67
OM10-25C-MG	*−6.66*	*1.81*	*32.73*	
	−6.72	*1.78*	*32.69*	
	−6.69	**1.80**	**32.71**	53–63
OM09-55C-MS	*−6.04*	*−6.95*	*23.70*	
	−6.07	*−7.04*	*23.60*	64–77
	−6.05	**−7.00**	**23.65**	
OM09-57C-MS	−9.10	−3.14	27.62	43–53
OM09-58C-MS	−10.00	−0.04	30.82	29–38
OM09-60C-MS	−7.74	5.56	36.59	7–15
OM09-61C-MS	−2.72	4.50	35.50	42–50
OM09-62C-MS	−7.38	3.53	34.50	46–55
OM09-63C-MS	−8.15	4.00	34.98	44–53
OM09-64C-MS	*−7.03*	*1.76*	*32.67*	
	−7.38	*2.20*	*33.13*	
	−7.21	**1.98**	**32.90**	53–62
OM09-50C-MS	−1.98	3.18	34.14	–
OM10-48C-MG	−7.57	−0.72	30.12	33–43
OM10-51C-MG	*−12.63*	*−4.50*	*26.22*	–
	−12.56	*−4.69*	*26.03*	
	−12.59	**−4.59**	**26.13**	–
OM10-52C-MG	*−7.72*	*−0.03*	*30.83*	
	−7.75	*0.10*	*30.96*	
	−7.74	**0.03**	**30.90**	62–73
OM10-54C-MG	*−7.37*	*2.48*	*33.42*	
	−7.43	*2.54*	*33.48*	
	−7.40	**2.51**	**33.45**	19–27
OM10-47C-MG-CLEAR	*−7.04*	*−3.86*	*26.88*	
	−7.07	*−3.80*	*26.94*	
	−7.05	**−3.83**	**26.91**	47–57
OM10-47C-MG-OPAQUE	*−3.35*	*1.44*	*32.35*	
	−3.50	*1.43*	*32.34*	
	−3.42	**1.44**	**32.34**	23–31
OM10-49C-MG	*−2.90*	*0.86*	*31.75*	
	−2.81	*0.96*	*31.85*	
	−2.85	**0.91**	**31.80**	25–33

Replicate analyses are indicated in italics, with the average of replicate analyses given in bold.

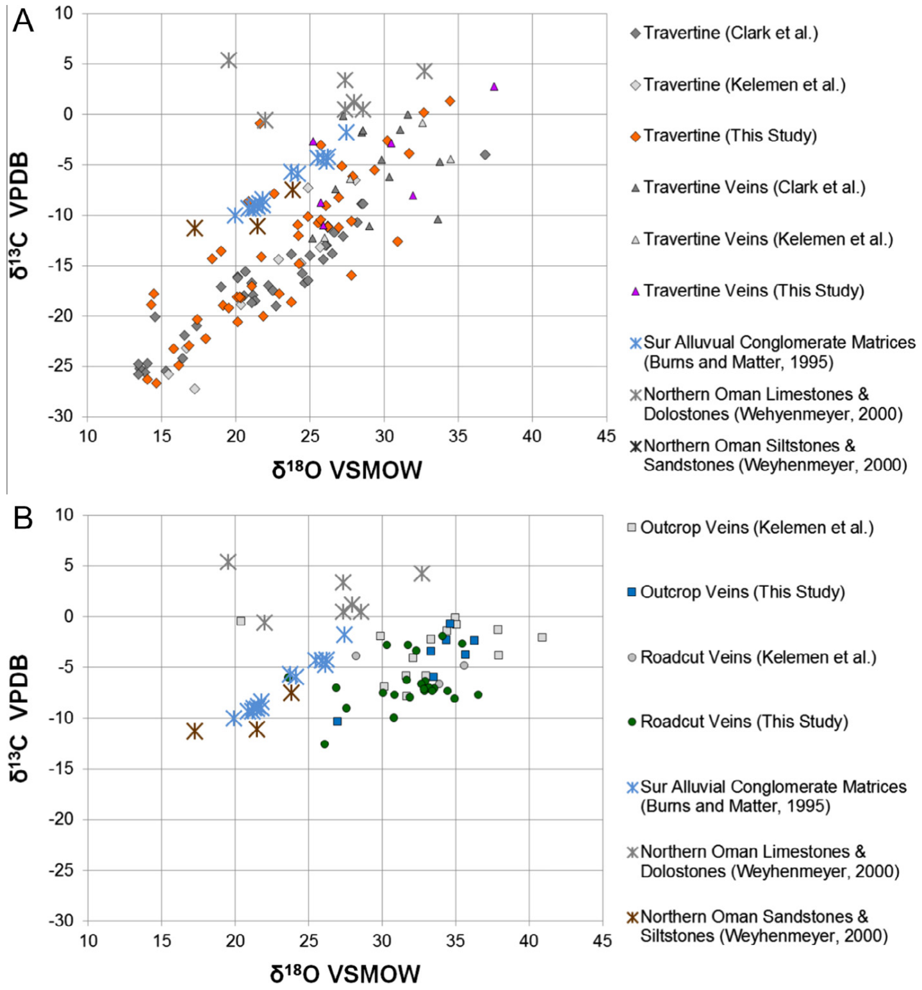

Fig. 9. Relation between $\delta^{13}C$ and $\delta^{18}O$ isotopic ratios for Samail carbonates. The isotopic data are expressed in delta notation relative to the Vienna Pee Dee Belemnite standard (VPDB) and the Vienna Mean Ocean Water standard (VSMOW). A: Ca-rich travertine veins (triangles) and surface travertine deposits (diamonds). B: Mg-rich carbonate outcrop veins (squares) and Mg-rich carbonate roadcut veins (circles). Data from this study (colored symbols); Kelemen and Matter (2008) and Kelemen et al. (2011) (light gray symbols); and Clark and Fontes (1990) and Clark et al. (1992) (dark gray symbols). Plotted for reference are isotopic values for Sur alluvial conglomerate carbonate matrices (blue stars) from Burns and Matter (1995) and for northern Oman limestones and dolostones (gray stars) as well as sandstones and siltstones (brown stars) from Weyhenmeyer (2000). (For interpretation of the references to color in this figure legend, the reader is referred to the web version of this article.)

travertines do extend to higher ratios. However, two of the surface travertine samples with higher $\delta^{13}C$ and $\delta^{18}O$ isotopic ratios (OM09-32C-MS-BROWN and OM10-28C-MG-BROWN) are brown, porous, weathered travertines that have anomalously young ^{14}C ages relative to adjacent samples, suggesting they have likely been affected by weathering and/or diagenesis.

6. DISCUSSION

6.1. Temporal and spatial trends in carbonate formation

6.1.1. Surface travertine deposition and preservation

The ages of the surface travertines indicate that travertine deposition and preservation has been ongoing for at least 50,000 years. The long-term preservation of the travertines is unusual compared to travertines formed in other ophiolites (e.g. Barnes and O'Neil, 1971; Flinn and Pentecost, 1995; Pentecost, 2005) and is likely a consequence of Oman's arid climate. Previously, Clark and Fontes (1990) argued that ^{14}C ages and C and O isotopic compositions for surface travertines and travertine veins in the Nizwa area indicate that there were alternating pluvial and hyperarid climatic periods in northern Oman, with surface travertines only deposited under hyperarid conditions and travertine veins (which they referred to as fracture calcites) primarily deposited during pluvial periods. Specifically, they argued for pluvial periods prior to 19,000 yr BP and from 6500 to 12,500 yr BP and for a hyperarid climate from 16,300 to 19,000 yr BP and from 6100 yr BP to the present day. However, the additional ^{14}C ages and C and O isotopic data obtained in this study and also by Kelemen et al. (Kelemen and Matter, 2008; Kelemen et al., 2011) fill in the gaps in the Clark and Fontes (1990) travertine dataset and suggest that travertine formation has been continuous over the past 50,000 years in northern Oman or at least that there are insufficient data to detect temporal or spatial variability in travertine deposition (Figs. 6, 7, and 9).

Although the overall ^{14}C age distributions do not support climate related episodic deposition of travertines, there is field evidence suggesting that travertine deposition has been episodic. At all four travertine locations investigated in this study, the travertine terraces are brown and weathered, and channels have cut through both the terraces as well as up to 1 to 2 m of the underlying peridotite bedrock (Fig. 3, Panels C and D, and Fig. 5, Panel A). The travertine terraces at these locations are primarily ~30,000 to 45,000 yr BP in age, and deposition of the modern travertines at these locations primarily occurs in the bottoms of the incised channels (Fig. 7). There may have been a time period of widespread travertine deposition that produced the ~1 to 2 m thick travertine terraces that was followed by a period or event of travertine erosion, which eroded the tops of some of the terraces and also created the incised channels. Subsequently, there was renewed deposition of travertine, primarily in the incised channels. However, there are not presently enough data to evaluate the specific nature and timing of episodic travertine deposition and erosion.

6.1.2. *Mg-rich carbonate veins*

The older ages of the Mg-rich carbonate veins relative to the Ca-rich carbonate veins are consistent with the concept that Type I waters deposit Mg-rich carbonates in the subsurface, become enriched in Ca as they evolve into Type II waters, and then deposit Ca-rich travertines at the surface (see Section 2). The Ca-rich carbonate veins are sampled near, and often underneath, layered travertine deposits and likely serve as feeder veins formed in the pathways of Type II waters towards the surface and/or formed by downward migration of Type II waters into cracks underlying the travertine terraces.

The presence of both older (^{14}C dead) and younger Mg-rich carbonate veins at roadcuts likely reflects open system behavior, at least relative to C, which has to be added from an external source. In order for the Mg-rich carbonate vein ages to be interpreted as formation ages, the assumption must be made that the C incorporated into the veins originated as atmospheric C. However, veins might undergo post-crystallization, open-system exchange with relatively ^{14}C-rich fluids, and this exchange could produce apparent ^{14}C ages that are younger than the initial formation ages. Alternatively, if the veins incorporated significant amounts of older C, then the apparent ^{14}C ages may be older than the formation ages. There are two possible sources of older C that could be incorporated into veins as they precipitate: (1) older carbonate veins, which could dissolve (fully or partially) and re-precipitate, thereby recycling older C and (2) the Tertiary to Precambrian carbonates (and also sandstones and siltstones with a carbonate component) located in the northern Oman mountains (e.g. Coleman, 1981; Weyhenmeyer, 2000), which authors such as Stephen et al. (2013) have argued could contribute significant older C if vein-forming fluids percolated through them.

Two lines of evidence suggest that the Samail carbonates have not incorporated significant older carbonate material from the Tertiary to Precambrian formations. First, the δ^{13}C, δ^{18}O, and ^{87}Sr/^{86}Sr values of the Samail carbonates are distinct from values measured in the Tertiary to Precambrian limestones, dolostones, sandstones, and siltstones and also from the carbonate matrices of alluvial conglomerates from Sur (Fig. 9; sediment data from Burns and Matter, 1995; Weyhenmeyer, 2000; also see Kelemen et al., 2011). The Sur conglomerate matrices were derived from waters that percolated through Maastrichtian to Tertiary carbonates and also through some Hawasina outcrops (Burns and Matter, 1995). While both the Sur samples and the Samail carbonates cover a wide range of δ^{13}C and δ^{18}O values, which are positively correlated, the δ^{13}C and δ^{18}O trend for the Sur carbonates is offset to higher values and is more closely aligned with the δ^{13}C and δ^{18}O values measured in the Tertiary to Precambrian carbonate and sandstone/siltstone rocks. The isotopic offset alone is not conclusive evidence because carbonate precipitating from the fluid dissolving the limestone may be isotopically different from the limestone itself. However, a second line of evidence is that fluids sampled from the Misht and Qafeefah Travertine locations have young ^{14}C ages ranging from >modern to a maximum of 680 ± 35 yr BP (Matter et al., 2012). These young ages indicate that the fluids contain mostly atmospheric CO_2 although a small amount of older C is likely incorporated into some of the alkaline springs. While we cannot rule out the possibility that this C comes from limestone terrain, a likely source of the C is older, local travertines that are being weathered. Furthermore, we do not observe significant amounts of older C in recent travertine precipitates from alkaline spring water (see Section 5.2.1). Therefore, we interpret the roadcut vein age distribution as representing multiple generations of carbonate vein formation, although the distribution of the apparent ages may have been affected by some open-system (dissolution and re-precipitation) behavior.

Approximately 50% of the Mg-rich carbonate roadcut veins analyzed in this study formed >50,000 yr BP. However, it is important to account for the bias introduced by the large number of ^{14}C dead veins from Fanja Roadcut, as discussed in Section 5.2.2. A locality-weighted average of veins dated from the three roadcut locations provides a lower value of 40% ^{14}C dead veins. Furthermore, despite analysis of numerous ($n = 28$) Mg-rich carbonate outcrop veins from 13 locations in the ophiolite (this study; also Kelemen and Matter, 2008; Kelemen et al., 2011), no ^{14}C dead samples have been observed on the natural peridotite weathering surface. An average which includes both outcrop and roadcut veins suggests that overall ~8% of Mg-rich carbonate veins are ^{14}C dead.

6.1.3. *Isotopic variability*

The surface travertines (Fig. 9, Panel A) exhibit generally lower δ^{13}C (−27 to 1.34‰) and δ^{18}O (14 to 34‰) values than the Mg-rich carbonate veins (Fig. 9, Panel B). The young travertines (<1000 yr BP) extend down to very low isotopic ratios of −27‰ δ^{13}C and <15‰ δ^{18}O (Fig. 10). Such low values have been attributed to kinetic fractionation effects resulting from rapid carbonate deposition in hyperalkaline pools (Clark et al., 1992; Wilson et al.,

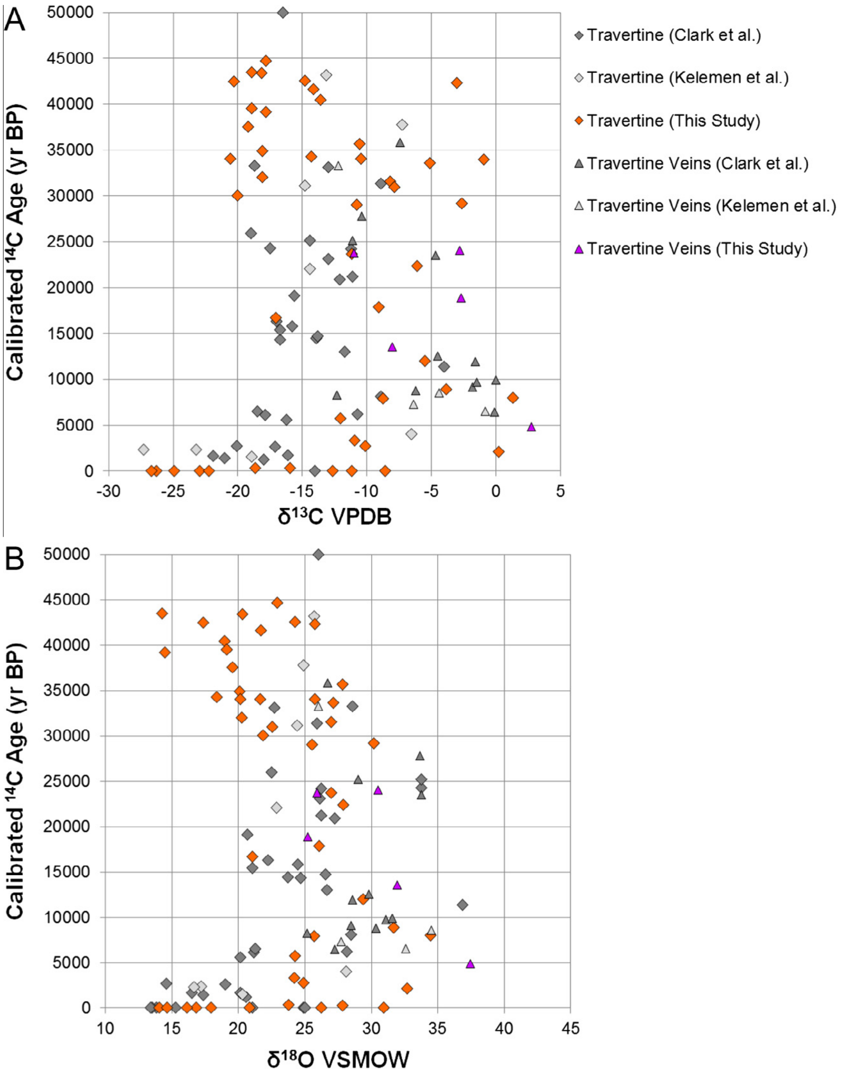

Fig. 10. Relation between ^{14}C age and δ^{13}C (Panel A) and δ^{18}O (Panel B) isotopic ratios for surface travertines (diamonds) and travertine veins (triangles) from the Samail Ophiolite. The isotopic data are expressed in delta notation relative to the Vienna Pee Dee Belemite standard (VPDB) and Vienna Standard Mean Ocean Water (VSMOW). Symbols and data sources as in Fig. 8A.

2010; Kelemen et al., 2011). Paukert et al. (2012)[3] report measurements of the pH for spring waters at the Qafeefah, Misht, Wadi Uqaybah, and Wadi Sudari travertines, all of which fall between 11.61 and 11.90. Such high pH values lead to rapid carbonate deposition and kinetic fractionation of both δ^{13}C and δ^{18}O, and this fractionation likely dominates over any isotopic fractionation due to evaporation (e.g. Clark et al., 1992; Wilson et al., 2010; Kelemen et al., 2011).

Data from this study increase the upper bound of δ^{13}C and δ^{18}O values in young travertines. Some young travertines that are composed predominantly of aragonite extend to values of −12‰ δ^{13}C and 32‰ δ^{18}O, suggesting different kinetic fractionation effects under the conditions of aragonite precipitation or, perhaps, biologically mediated precipitation (e.g. McConnaughey, 1989a,b; Power et al., 2011).

While showing considerable scatter, the older (>1000 yr BP) travertines generally have higher isotopic ratios than the young travertines. Several studies (Clark et al., 1992; Kelemen et al., 2011) suggest diagenetic and/or re-crystallization processes (that occur under slower conditions in equilibrium with fresher wadi waters) to account for the higher isotopic ratios in older samples. An alternative hypothesis proposed by Clark and Fontes (1990) and Clark et al. (1992) is that in the past during less arid conditions when there would have been higher water/rock ratios, the pH of the hyperalkaline springs was lower, reducing the strength of kinetic fractionation processes. The new data from this study indicate that there are a few samples with ages from ~39,000 to 45,000 yr BP that have isotopic ratios

---

[3] Note that the "Qafifah" site in Paukert et al. (2012) is the same as the "Qafeefah" site in this study. In addition, the "Al Bana" site in Paukert et al. (2012) is the same as the "Misht" site in this study. Al Bana is the name of the closest village to Misht Travertine.

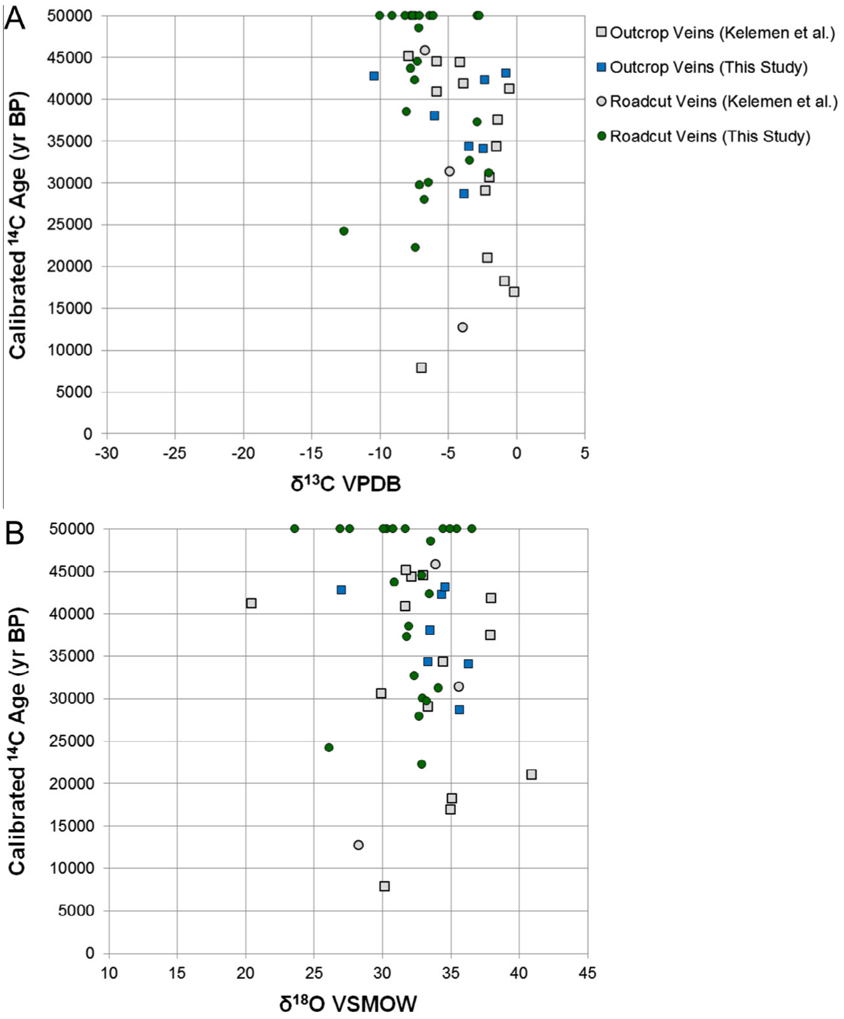

Fig. 11. Relation between ^{14}C age and δ^{13}C (Panel A) and δ^{18}O (Panel B) isotopic ratios for Mg-rich outcrop (square) and roadcut (circles) carbonate veins from the Samail Ophiolite. The isotopic data are expressed in delta notation relative to the Vienna Pee Dee Belemite standard (VPDB) and Vienna Standard Mean Ocean Water (VSMOW). Symbols and data sources as in Fig. 8B.

(most notably δ^{18}O, see Fig. 10) as low as the young travertines. These data are consistent with the hypothesis that the conditions leading to the extreme kinetic fractionation observed in modern travertine precipitates also occurred during periods in the past.

There are no obvious systematic relationships between age and δ^{13}C and δ^{18}O ratios for the Mg-rich carbonate veins (Fig. 11) nor any differences between the outcrop and roadcut veins. It is possible that the magnesite in these veins formed by dehydration of a hydrated carbonate precursor and that the isotopic ratios reflect that process rather than precipitation of magnesite. However, no hydromagnesite or other hydrated Mg-carbonate phase that would allow evaluation of the impact of dehydration on the stable isotopic ratios was detected in the XRD analyses of the Mg-rich carbonate vein samples.

The Mg-rich carbonate outcrop veins cover a broad range of δ^{13}C (−10 to −0.2‰) and δ^{18}O (20 to 41‰) values with no obvious temporal trends. The ^{14}C dead roadcut veins cover a broad range of both δ^{13}C (−12 to −2‰) and δ^{18}O (23 to 37‰) whereas the roadcut veins <50,000 yr BP have a similar range of δ^{13}C (−8 to −3‰) but a much narrower range of δ^{18}O (all but one sample fall in the range of 32 to 33‰). This may indicate that during the last 50,000 years the fluids from which the carbonate veins deposited had similar isotopic characteristics, and the conditions of precipitation were similar. Since the ages of the ^{14}C dead samples are unknown, they may represent carbonates formed over a much longer period of time under different conditions and from fluids of different origins.

6.2. Carbonate formation temperatures

Most of the handpicked carbonate samples are composed primarily of a single carbonate mineral, so the δ^{18}O value of the whole rock represents a close approximation of the δ^{18}O value for the dominant mineral. For these samples, approximate temperatures of formation can be estimated by assuming that the carbonates formed in equilibrium with typical Oman groundwaters and hyperalkaline spring waters, which have δ^{18}O values ranging from −2‰ to 1‰ (Neal and Stanger, 1985; Clark et al., 1992;

Matter et al., 2006; Kelemen et al., 2011). Formation temperatures can be calculated for the minerals calcite, dolomite, and magnesite using equilibrium exchange formulas in O'Neil et al. (1969), Friedman and O'Neil (1977), Schauble et al. (2006), and Chacko and Deines (2008) after corrections of magnesite and dolomite isotopic measurements for fractionation during dissolution in phosphoric acid at 77 °C using the equations given in Das Sharma et al. (2008). Calculated equilibrium formation temperatures are presented in Table 3.

The dolomite (all veins except for one channel-filling travertine) and magnesite (all veins) samples suggest relatively low temperatures of formation. The dolomites have equilibrium formation temperatures ranging from approximately 20 to 60 °C while the magnesite samples fall within a tighter range of approximately 40 to 60 °C. There is no significant difference in the temperatures of formation between outcrop and roadcut veins or between ^{14}C dead and younger veins. The relatively low formation temperatures of the dolomite and magnesite subsurface veins are generally consistent with the hypotheses of Kelemen and Matter (2008), Kelemen et al. (2011), and Streit et al. (2012) that these veins were formed in a relatively shallow weathering horizon.

The modern ambient temperature in northern Oman ranges from approximately 20 to 40 °C. Therefore, the upper temperatures calculated for the dolomite and magnesite veins indicate formation of some veins at depth. Using a geothermal gradient for northern Oman of ~30 °C km^{-1} (Gunnell et al., 2007), these Mg-rich veins could potentially have formed at 0.5 to 1 km depth. This is consistent with the observation of Neal and Stanger (1985) of geothermally heated hyperalkaline spring waters that range in temperature from 21 to 41 °C. On average, these spring waters are 4.3 °C warmer than associated surface stream waters but there are some that are up to ~15 °C warmer. Assuming a geothermal gradient of 20 °C km^{-1} and isotropic conditions, Neal and Stanger (1985) argued that hyperalkaline spring waters may circulate as deep as 0.7 km in the peridotite layer of the ophiolite.

The calcite-rich travertines provide a large range of temperatures from unrealistically high values of 100 to 120 °C (for recently-formed precipitates and also for a few older samples from Wadi Sudari Travertine) to unrealistically low values of 0 °C. Approximately 60% of the samples have formation temperatures ranging from 20 to 60 °C. The anomalous formation temperatures may reflect the impact of kinetic fractionation on both C and O isotopes. For example, the recently-formed precipitates have experienced significant kinetic fractionation of both C and O isotopes. Formation temperatures were also calculated for three calcite-rich travertine veins. Only one sample (OM10-13P-MG) provides a realistic formation temperature around 30 °C. The other two samples give anomalously low and unrealistic temperatures suggesting that, contrary to the conclusion of Clark and Fontes (1990), the travertine veins do not form in equilibrium with surface waters.

6.3. Estimating natural rates of carbonate formation in Samail Peridotite

6.3.1. Travertine deposition rates

Based on the thicknesses and ages of layers within travertine terraces (see Supplementary Information), we have calculated deposition rates of ~0.1 mm/yr for the time period ~29,000 to 45,000 yr BP at Misht Travertine and ~0.3 mm/yr for the time period ~30,000 to 42,000 yr BP at Wadi Uqaybah Travertine. In addition, we have calculated deposition rates of ~0.005 mm/yr for pseudospeleothem growth at Wadi Sudari Travertine for the time period ~34,000 to 43,000 yr BP. The precipitation rates for the pseudospeleothem are likely slower because it was formed through dripping and evaporation rather than by direct precipitation in an alkaline pool. Compared with deposition rates for other types of travertines (Table 4), the Samail travertines deposit relatively slowly and their precipitation rates are most similar to speleothem travertine deposition rates.

Neal and Stanger (1985) note the locations of approximately 50 hyperalkaline springs, and Kelemen and Matter (2008) estimate that there are about 45 travertine deposits in the ophiolite based on detailed mapping in the southern third of the ophiolite. Using an estimate of total travertine area in the Samail Ophiolite of ~10^7 m^2 (Kelemen and Matter, 2008) and the travertine deposition rate of ~0.1 to 0.3 mm/yr for travertine terraces with ages between ~30,000 and 45,000 yr BP, ~1000 to 3000 m^3/yr of travertine was deposited in the Samail Ophiolite during that time, sequestering ~1 to 3 × 10^6 kg CO_2/yr. The measured travertine deposition rates are strikingly similar to the rate obtained by dividing the average thickness of travertine (~2 m including some of the "travertine veins") by the average age of travertines (~25,000 years), yielding ~0.1 mm/yr (also see Kelemen et al., 2011), suggesting that

Table 4
Travertine deposition rates.

Type of travertine	Deposition rate (mm/yr)	Average deposition rate (mm/yr)	Data source
Misht Travertine Sequence	0.1	–	This study
Wadi Uqaybah Travertine Sequence #1	0.3	–	This study
Wadi Uqaybah Travertine Sequence #2	0.3	–	This study
Wadi Sudari Pseudospeleothem	0.005	–	This study
Epigean Meteogene (All)	0.04–48	5.28 ($n = 55$)	Pentecost (2005)
Cyanobacteria-Associated	0.04–7.0	2.38 ($n = 16$)	Pentecost (2005)
Eukaryotic Algae-Associated	0.42–48	9.08 ($n = 5$)	Pentecost (2005)
Bryophyte-Associated	0.6–20	8.7 ($n = 7$)	Pentecost (2005)
Speleothem	0.002–0.90	0.027 ($n = 8$)	Pentecost (2005)
Thermogene	1–1000	202 ($n = 16$)	Pentecost (2005)

the deposition rate is approximately constant on time scales of 10,000 to 15,000 years.

Today, travertine deposition does not occur simultaneously over the total area of exposed travertine. Rather, travertine deposition directly on the surface is limited to a few millimeters or centimeters per year within a few tens of meters of the hyperalkaline springs found at each travertine deposit. The hyperalkaline springs that precipitate travertines also migrate over the surface of the travertine with time (e.g. Neal and Stanger, 1985; Kelemen and Matter, 2008). In addition, crosscutting veins (e.g. Fig. 4 in Kelemen and Matter, 2008) demonstrate that there is precipitation of travertine within travertine terraces, the rate of which probably varies with space and time. Therefore, at any given time, travertine is likely being precipitated over a fraction of the total travertine area. However, the agreement between the outcrop measured rates and the average rate of deposition of travertines suggests that the entire surface grows at approximately the same rate when averaged over 10,000 to 20,000 years. Thus, we concur with Kelemen and Matter (2008) that the ages of the travertines reflect a balance between slow deposition and slow erosion, which has removed most travertine samples older than 50,000 years.

6.3.2. Natural CO_2 sequestration in Mg-rich carbonate veins

The discovery of a significant number of ^{14}C dead Mg-rich carbonate veins at roadcuts allows us to place further constraints on the natural rate of CO_2 uptake in carbonate veins that was estimated by Kelemen and Matter (2008). That estimate was based on an average vein age of 26,000 yr BP (and a maximum vein age of 50,000 yr BP) and the assumption that the carbonate veins were primarily deposited in a shallow weathering zone ~15 m thick. This resulted in an estimate of $\sim 10^{12}$ kg of CO_2 stored in subsurface carbonate veins in the peridotite layer of the Samail Ophiolite, yielding a natural uptake rate of $\sim 4 \times 10^7$ kg CO_2/yr.

However, the depth of the peridotite weathering zone containing the Mg-rich carbonate veins is uncertain. The weathering horizon is at least ~5 to 10 m based on the heights of roadcuts exposing carbonate veins. The thickness of the weathering zone of ~15 m estimated by Kelemen and Matter (2008) was based both on physical mass balance considerations that assume that weathering of the ophiolite keeps pace with erosion of the ophiolite and on chemical mass balance calculations that indicate that the travertine/subsurface vein ratio should be ~10. However, as discussed in Section 6.2, temperatures of hyperalkaline spring water (Neal and Stanger, 1985) and isotopic data from vein carbonates (this study) suggest that the peridotite weathering zone could be as deep as 0.5 to 1 km, although the extent of carbonation at such depths is unknown.

Fig. 12 examines the impact of the presence of ^{14}C dead subsurface carbonate veins and the depth of the peridotite weathering horizon on estimates of natural CO_2 sequestration rates. It suggests that Mg-rich carbonate vein formation in the peridotite layer of the Samail Ophiolite consumes an estimated 10^7 to 10^8 kg CO_2/yr, which is within the range of, or greater than, the estimate of Kelemen and Matter (2008). It is notable that at shallow depths of weathering, the CO_2 uptake rates are not very sensitive to the percentage of ^{14}C dead carbonate veins. Further refinement of estimates for the natural CO_2 uptake rate will require both better constraints on the ages of veins, especially those older than 50,000 years, from a broadened set of sampling locations and improved estimates of the thickness of the peridotite weathering zone.

6.3.3. Samail peridotite carbonation in a global context

Constraining the natural carbonation rate of ultramafic rocks is important in order to assess the role of this carbonation in the global carbon cycle. Significant ophiolite belts are found in the United States, Europe, the Middle East, China, Japan, Papua New Guinea, Indonesia, New Caledonia, and eastern South America, and ophiolites have been estimated to cover ~1% of the total continental surface (e.g. Coleman, 1977; Dilek and Furnes, 2011). Extrapolating the estimated CO_2 sequestration rate of

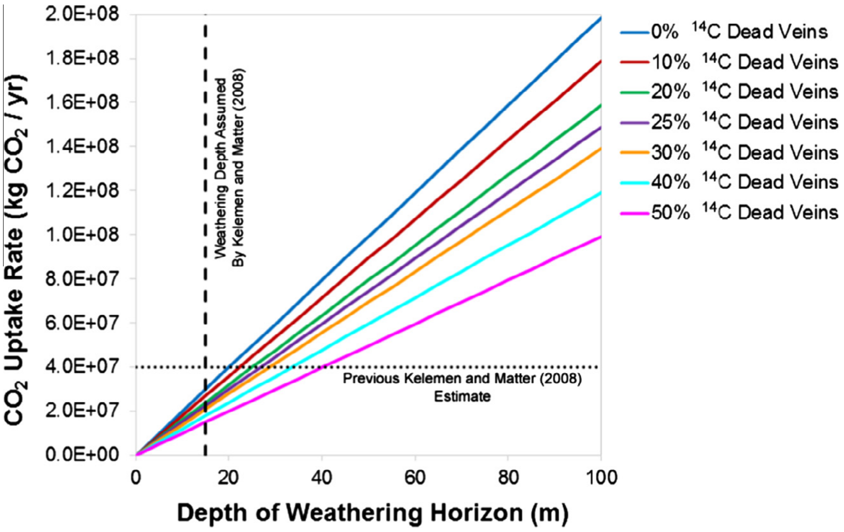

Fig. 12. Sensitivity analysis illustrating the variation of CO_2 uptake rates as a function of the depth of the weathering horizon and the percentage of ^{14}C dead subsurface veins in the Samail Ophiolite.

~10^7 kg CO_2/yr for Mg-rich carbonate veins in the Samail Ophiolite suggests the potential for ~4×10^9 kg CO_2/yr to be sequestered globally in subaerial exposures of peridotite. There may also be significant carbonate formation in seafloor exposures of peridotite, particularly at slow-spreading ridges, where it is estimated that peridotites comprise ~50% of the rocks exposed (Escartin et al., 2008). For example, carbonates have been forming for the past ~100,000 years at the off-axis Lost City peridotite-hosted hydrothermal field (30°N, Mid-Atlantic Ridge) (e.g. Ludwig et al., 2011). However, the total volume of exposed seafloor peridotites is very poorly constrained.

The order of magnitude estimate of CO_2 sequestered through natural carbonation of subaerial exposures of peridotite is small relative to the estimated 1.5 to 1.8×10^{11} -kg CO_2/yr sequestered by chemical weathering of both terrestrial and seafloor basalt (e.g. Staudigel et al., 1989; Alt and Teagle, 1999; Dessert et al., 2003). It is also several orders of magnitude less than the estimated 35×10^{12} kg of anthropogenic CO_2 emitted in 2010 (Friedlingstein et al., 2010). However, it is larger than both the estimated 6.3×10^6 kg CO_2/yr sequestered in chrysotile mine tailings at Clinton Creek, Yukon Territory, Canada (Wilson et al., 2006, 2009a,b), and the 10^6 kg of CO_2 that was recently injected into a basalt formation near Wallula, Washington as part of the Big Sky Carbon Sequestration Partnership pilot project to test long-term carbon storage in basalt (http://www.bigskyco2.org/research/geologic/basaltproject).

7. SUMMARY

New ^{14}C ages and stable C and O isotope analyses for carbonates produced through alteration of the mantle peridotite layer of the Samail Ophiolite, Sultanate of Oman, support the hypothesis (e.g. Kelemen and Matter, 2008) that these carbonates are primarily formed as a result of recent, low-temperature, near-surface alteration of the peridotite. Deposition of Ca-rich travertines from hyperalkaline springs is ongoing and has been occurring more or less continuously over the past ~50,000 yr BP. Ca-rich carbonate veins associated with travertine deposits range in age from ~4,000 to 36,000 yr BP (average age: 15,000 yr BP). Detailed subsampling of travertine terraces indicates that travertine deposition rates were ~0.1 to 0.3 mm/yr between 30,000 and 45,000 yr BP. Using an estimate of total travertine area from Kelemen and Matter (2008), a maximum of ~1000 to 3000 m^3/yr of travertine was deposited in the Samail Ophiolite during this time period, sequestering ~1 to 3×10^6 kg CO_2/yr in surface deposits. As noted by Kelemen and Matter (2008) and Kelemen et al. (2011), formation of these surface deposits was probably accompanied by subsurface formation of 2.5 times this amount in Ca-rich carbonate veins.

^{14}C ages of Mg-rich carbonate veins exposed on the natural peridotite weathering surface indicate that these veins formed ~8000 to 45,000 yr BP (average age: 35,000 yr BP). However, dating of less-weathered veins from three roadcuts has also demonstrated that there are a significant number of Mg-rich carbonate veins that are older than 50,000 years. A locality-weighted average suggests that approximately 40% of Mg-rich carbonate veins sampled at three roadcuts are ^{14}C dead. The new ^{14}C vein ages allow us to further constrain natural rates of CO_2 sequestration in subsurface Mg-rich carbonate veins to ~10^7 kg CO_2/yr, in agreement with Kelemen and Matter (2008) and Kelemen et al. (2011) and depending on the proportion of ^{14}C dead veins and the thickness of the weathering zone in which the veins are forming. Further refinement of this carbonation rate will require a better understanding of the age distributions of Mg-rich carbonate veins and also the thickness of the peridotite weathering zone. Global subaerial exposures of peridotite could potentially sequester on the order of 10^9 kg CO_2/yr.

ACKNOWLEDGMENTS

Ali Al-Rajhi, Ministry of Commerce and Industry, Sultanate of Oman, and Sobhi Nasir, Sultan Qaboos University, are thanked for logistical support during field seasons. Jürg Matter, Everett Shock, Lisa Streit, Amelia Paukert, Jackie Gauntlett, and other members of the Oman field teams are thanked for assistance with fieldwork and for scientific discussions. Jerzy Blustajn, Margaret Sulanowska, Lora Wingate, Karen Benedetto, Chris Weidman, Ann McNichol, Mark Roberts, and Steve Richardson are thanked for mentorship in the laboratory and assistance with sample preparation and labwork. This research was funded by National Science Foundation grants EAR-1049281 and EAR-1049905, the Deep Ocean Exploration Institute at Woods Hole Oceanographic Institution, the Academic Programs Office at Woods Hole Oceanographic Institution, the Mellon Foundation, a Research Initiative in Science and Engineering Grant from Columbia University to Peter Kelemen and Jürg Matter, and Peter Kelemen's Arthur D. Storke Chair at Columbia University. Siobhan A. Wilson, an anonymous reviewer, and Frank McDermott (Associate Editor) are thanked for thoughtful comments that greatly improved the paper.

APPENDIX A. SUPPLEMENTARY DATA

Supplementary data associated with this article can be found, in the online version, at http://dx.doi.org/10.1016/j.gca.2013.11.007.

REFERENCES

Akbulut M., Piskin O. and Karayigit A. I. (2006) The genesis of the carbonatized and silicified ultramafics known as listwanites: A case study from the Mihalıççık region (Eskişehir), NW Turkey. *Geol. J.* **41**, 557–580.

Alt J. C. and Teagle D. A. H. (1999) The uptake of carbon during alteration of oceanic crust. *Geochim. Cosmochim. Acta* **63**, 1527–1535.

Barnes I. and O'Neil J. R. (1969) The relationship between fluids in some fresh Alpine type ultramafics and possible modern serpentinization, Western United States. *Geol. Soc. Amer. Bull.* **80**, 1947–1960.

Barnes I. and O'Neil J. R. (1971) Calcium-magnesium carbonate solid solutions from Holocene conglomerate cements and travertines in the Coast Range of California. *Geochim. Cosmochim. Acta* **35**, 699–718.

Barnes I., LaMarche V. C. and Himmelberg G. (1967) Geochemical evidence of present day serpentinization. *Science* **156**, 830–832.

Barnes I., O'Neil J. R. and Trescases J. J. (1978) Present-day serpentinization in New Caledonia, Oman, and Yugoslavia. *Geochim. Cosmochim. Acta* **42**, 144–145.

Beinlich A. and Austrheim H. (2012) *In situ* sequestration of atmospheric CO_2 at low temperature and surface cracking of serpentinized peridotite in mine shafts. *Chem. Geol.* **332–333**, 32–44.

Beinlich A., Plümper O., Hövelmann J., Austrheim H. and Jamtveit B. (2012) Massive serpentinite carbonation at Linnajavri, N-Norway. *Terra Nova* **24**, 446–455.

Boaretto E., Bryant C., Carmi I., Cook G., Gulliksen S., Harkness D., Heinemeier J., McClure J., McGee E., Naysmith P., Possnert G., Scott M., van der Plicht H. and van Strydonck M. (2002) Summary findings of the fourth international radiocarbon intercomparison (FIRI) (1998–2001). *J. Quaternary Sci.* **17**, 633–637.

Boschi C., Dini A., Dallai L., Ruggieri G. and Gianelli G. (2009) Enhanced CO_2-mineral sequestration by cyclic hydraulic fracturing and Si-rich fluid infiltration into serpentinites at Malentrata (Tuscany, Italy). *Chem. Geol.* **265**, 209–226.

Bruni J., Canepa M., Chiodini G., Cioni R., Cipolli F., Longinelli A., Marini L., Ottonello G. and Zuccolini M. V. (2002) Irreversible water-rock mass transfer accompanying the generation of the neutral, Mg-HCO_3 and high-pH, Ca-OH spring waters of the Genova province, Italy. *Appl. Geochem.* **17**, 455–474.

Burke A., Robinson L. F., McNichol A. P., Jenkins W. J., Scanlon K. M. and Gerlach D. S. (2010) Reconnaissance dating: A new radiocarbon method applied to assessing the temporal distribution of Southern Ocean deep-sea corals. *Deep-Sea Res. Pt. I* **57**, 1510–1520.

Burns S. J. and Matter A. (1995) Geochemistry of carbonate cements in surficial alluvial conglomerates and their paleoclimatic implications. *J. Sediment. Res.* **A65**(1), 170–177.

Chacko T. and Deines P. (2008) Theoretical calculation of oxygen isotope fractionation factors in carbonate systems. *Geochim. Cosmochim. Acta* **72**, 3642–3660.

Chizmeshya A. V. G., McKelvy M. J., Squires K., Carpenter R. W. and Bérat H. (2007) A novel approach to mineral carbonation: Enhancing carbonation while avoiding mineral pretreatment costs. U.S. Department of Energy Final Report 924162, Tempe, Arizona, Arizona State University.

Cipolli F., Gambardella B., Marini L., Otonello G. and Zuccolini M. V. (2004) Geochemistry of high-pH waters from serpentinites of the Gruppo di Voltri (Genova, Italy) and reaction path modeling of CO_2 sequestration in serpentine aquifers. *Appl. Geochem.* **19**, 787–802.

Clark I. D. and Fontes J.-C. (1990) Paleoclimate reconstruction in northern Oman based on from hyperalkaline groundwaters. *Quat. Res.* **33**, 320–336.

Clark I. D., Fontes J.-C. and Fritz P. (1992) Stable isotope disequilibria in travertine from high pH waters: Laboratory investigations and field observations from Oman. *Geochim. Cosmochim. Acta* **56**, 2041–2050.

Coleman R. G. (1977) Ophiolites. Springer-Verlag, New York.

Coleman R. G. (1981) Tectonic setting for ophiolite obduction in Oman. *J. Geophys. Res.* **86**, 2497–2508.

Das Sharma S., Patil D. J. and Gopalan K. (2008) Temperature dependence of oxygen isotope fractionation of CO_2 from magnesite-phosphoric acid reaction. *Geochim. Cosmochim. Acta* **66**, 589–593.

Dessert C., Dupré B., Françoise L. M., Schott J., Gaillardet J., Chakrapani G. and Bajpai S. (2001) Erosion of Deccan Traps determined by river chemistry: Impact on the global climate and the $^{87}Sr/^{86}Sr$ ratio of seawater. *Earth Planet. Sci. Lett.* **188**, 459–574.

Dessert C., Dupré B., Gaillardet J., François L. and Allègre C. (2003) Basalt weathering laws and the impact of basalt weathering on the global carbon cycle. *Chem. Geol.* **202**, 257–273.

Dewandel B., Lachassagne P., Bakalowicz M., Weng P. and Al-Malki A. (2003) Evaluation of aquifer thickness by analyzing recession hydrographs: Application to the Oman ophiolite hard-rock aquifer. *J. Hydrol.* **274**, 248–269.

Dewandel B., Lachassagne P. and Qatan A. (2004) Spatial measurements of stream baseflow, a relevant method for aquifer characterization and permeability evaluation: Application to a hard rock aquifer, Oman ophiolite. *Hydrol. Process.* **18**, 3391–3400.

Dewandel B., Lachassagne P., Boudier F., Al-Hattali S., Ladouche B., Pinault J.-L. and Al-Suleimani Z. (2005) A conceptual and hydrogeological model of ophiolite hard-rock aquifers in Oman based on a multiscale and multidisciplinary approach. *Hydrogeol. J.* **13**, 708–726.

Dilek Y. and Furnes H. (2011) Ophiolite genesis and global tectonics: Geochemical and tectonic fingerprinting of ancient oceanic lithosphere. *Geol. Soc. Am. Bull.* **123**, 61–69.

Escartin J., Smith D., Cann J., Schouten H., Langmuir C. and Escrig S. (2008) Central role of detachment faults in accretion of slow-spreading oceanic lithosphere. *Nature* **455**, 790–794.

Ferry J. M. (1995) Fluid-flow during contact-metamorphism of ophicarbonate rocks in the Bergell-Aureole, Val-Malenco, Italian Alps. *J. Petrol.* **36**, 1039–1053.

Flinn D. and Pentecost A. (1995) Travertine-cemented screes on the serpentinite seacliffs of Unst and Fetlar, Shetland. *Mineral. Mag.* **59**, 259–265.

Friedlingstein P., Houghton R. A., Marland G., Hackler J., Boden T. A., Conway T. J., Canadell J. G., Raupach M. R., Ciais P. and Le Quéré C. (2010) Update on CO_2 emissions. *Nat. Geosci.* **3**, 811–812.

Friedman I. and O'Neil J. R. (1977) Compilation of stable isotope factors of geochemical interest. In *USGS Professional Paper 440-KK, Data of Geochemistry* (ed. M. Fleischer). U.S. Geological Survey, Reston, VA, pp. KK1–KK12.

Früh-Green G. L., Kelley D. S., Bernasconi S. M., Karson J. A., Ludwig K. A., Butterfield D. A., Boschi C. and Proskurowski G. (2003) 30,000 years of hydrothermal activity at the Lost City vent field. *Science* **301**, 495–498.

Glennie K. W., Bouef M. G. A., Hughes-Clark M. W., Moody-Stuart M., Pilaar W. F. H. and Reinhardt B. M. (1973) Late Cretaceous nappes in the Oman mountains and their geological evolution. *Am. Assoc. Pet. Geol. Bull.* **57**, 5–27.

Glennie K. W., Bouef M. G. A., Hughes-Clark M. W., Moody-Stuart M., Pilaar W. F. H. and Reinhardt B. M. (1974) Geology of the Oman mountains. *Verh. K. Ned. Geol. Mijnbouwk. Genoot.* **31**, 423.

Goldberg D. S., Takahashi T. and Slagle A. L. (2008) Carbon dioxide sequestration in deep-sea basalt. *Proc. Natl. Acad. Sci. U.S.A.* **105**, 9920–9925.

Gunnell Y., Carter A., Petit C. and Fournier M. (2007) Post-rift downwarping at passive margins: New insights from southern Oman using stratigraphy to constrain apatite fission-track and (U-Th)/He dating. *Geology* **35**, 647–650.

Halls C. and Zhao R. (1995) Listvenite and related rocks: Perspectives on terminology and mineralogy with reference to an occurrence at Cregganbaun, Co. Mayo, Republic of Ireland. *Mineral. Deposita* **30**, 303–313.

Hansen L. D., Dipple G. M., Gordon T. M. and Kellet D. A. (2005) Carbonated serpentinite (listwanite) at Atlin, British Columbia: A geological analogue to carbon dioxide sequestration. *Can. Mineral.* **43**, 225–239.

Harrison A. L., Power I. M. and Dipple G. M. (2013) Accelerated carbonation of brucite in mine tailings for carbon sequestration. *Environ. Sci. Technol.* **47**, 126–134.

Ivany L. C., Lohmann K. C., Blake D. B., Aronson R. B., Hasiuk F., Glass A. and Moody R. M. (2008) Eocene climate record of a high southern latitude continental shelf and implications for the biota: Seymour Island, Antarctica. *Geol. Soc. Amer. Bull.* **120**, 659–678.

Karlen I., Olsson I. U., Kallburg P. and Kilici S. (1964) Absolute determination of the activity of two ^{14}C dating standards. *Arkiv Geofysik* **4**, 465–471.

Kelemen P. B. and Matter J. M. (2008) *In situ* carbonation of peridotite for CO_2 storage. *Proc. Natl. Acad. Sci. U.S.A.* **105**, 17295–17300.

Kelemen P. B., Matter J. M., Streit E. E., Rudge J. F., Curry W. B. and Blusztajn J. (2011) Rates and mechanisms of mineral carbonation in peridotite: Natural processes and recipes for enhanced, *in situ* CO_2 capture and storage. *Ann. Rev. Earth Planet. Sci.* **39**, 545–576.

Kelley D. S., Karson J. A., Blackman D. K., Früh-Green G. L., Butterfield D. A., Lilley M. D., Olson E. J., Schrenk M. O., Roe K. K., Lebon G. T. and Rivizzigo P. (2001) An off-axis hydrothermal vent field near the Mid-Atlantic Ridge at 30 degrees N. *Nature* **412**, 145–149.

Lackner K. S. (2002) Carbonate chemistry for sequestering fossil carbon. *Annu. Rev. Energ. Env.* **27**, 193–232.

Lackner K. S., Wendt C. H., Butt D. P., Joyce E. L. and Sharp D. H. (1995) Carbon dioxide disposal in carbonate minerals. *Energy* **20**, 1153–1170.

Lippard SJ., Shelton A. W. and Gass I. G. (1986). *The ophiolite of Northern Oman*. .

Ludwig K. A., Kelley D. S., Butterfield D. A., Nelson B. K. and Früh-Green G. L. (2006) Formation and evolution of carbonate chimneys at the Lost City hydrothermal field. *Geochim. Cosmochim. Acta* **70**, 3625–3645.

Ludwig K. A., Shen C.-C., Kelley D. S., Cheng H. and Edwards L. R. (2011) U-Th systematics and ^{230}Th ages of carbonate chimneys at the Lost City hydrothermal field. *Geochem. Cosmochim. Acta* **75**, 1869–1888.

Matter J. M. and Kelemen P. B. (2009) Permanent storage of carbon dioxide in geological reservoirs by mineral carbonation. *Nat. Geosci.* **2**, 837–841.

Matter J. M., Waber H. N., Loew S. and Matter A. (2006) Recharge areas and geochemical evolution of groundwater in an alluvial aquifer system in the Sultanate of Oman. *Hydrogeol. J.* **14**, 203–224.

Matter J. M., Kelemen P. B., Paukert A., Mervine E. M. and Shock E. (2012) Geochemical constraints on in situ mineral carbonation of mantle peridotite in the Samail Ophiolite, Oman. International Conference on the Geology of the Arabian Plate and the Oman Mountains, Sultan Qaboos University, Muscat, Oman, January 7th–9th (abstr.).

McConnaughey T. (1989a) ^{13}C and ^{18}O isotopic disequilibrium in biological carbonates: I. Patterns. *Geochim. Cosmochim. Acta* **53**, 151–162.

McConnaughey T. (1989b) ^{13}C and ^{18}O isotopic disequilibrium in biological carbonates: II. In vitro simulation of kinetic isotope effects. *Geochim. Cosmochim. Acta* **53**, 163–171.

McNichol A. P., Gagnon A. R., Osborne E. A., Hutton D. L., von Reden K. F. and Schneider R. J. (1995) Improvements in procedural blanks at NOSAMS: Reflections of improvements in sample preparation and accelerator operation. *Radiocarbon* **37**, 683–691.

Nasir S., Al-Sayigh A. R., Al-Harthy A., Al-Kirbash S., Al-Jaaidi O., Musllam A., Al Mishwat A. and Al-Bu'saidi S. (2007) Mineralogical and geochemical characterization of listwaenite from the Semail Ophiolite, Oman. *Chem. Erde* **67**, 213–228.

Neal C. and Stanger G. (1983) Hydrogen generation from mantle source rocks in Oman. *Earth Planet. Sci. Lett.* **66**, 315–320.

Neal C. and Stanger G. (1984) Calcium and magnesium-hydroxide precipitation from alkaline groundwaters in Oman, and their significance to the process of serpentinization. *Mineral. Mag.* **48**, 237–241.

Neal C. and Stanger G. (1985) Past and present serpentinization of ultramafic rocks: An example from the Semail ophiolite nappe of northern Oman. In *The Chemistry of Weathering* (ed. J. I. Drewer). D. Reidel Publishing Company, Holland, pp. 249–275.

Nicolas A., Boudier F., Ildefonse V. and Ball E. (2000) Accretion of Oman and United Arab Emirates ophiolite—Discussion of a new structural map. *Mar. Geophys. Res.* **21**, 147–149.

O'Connor W. K., Dahlin D. C., Rush G. E., Gerdemann S. J. and Neilsen D. N. (2004) Aqueous mineral carbonation. U.S Department of Energy Final Report DOE/ARC-TR-04-002, U.S. Department of Energy, Albany Research Center, Albany.

Olsson I. U. (1970) The use of oxalic acid as a standard. In *Radiocarbon Variations and Absolute Chronology, Nobel Symposium, 12th Proceedings*. John Wiley and Sons, New York, pp. 17 (abstr.).

O'Neil J. R., Clayton R. N. and Mayeda T. K. (1969) Oxygen isotope fractionation in divalent metal carbonates. *J. Chem. Phys.* **51**, 5547–5558.

Pallister J. S. and Hopson C. A. (1981) Samail Ophiolite plutonic suite: Field relations, phase variation, cryptic variation and layering, and a model of a spreading ridge magma chamber. *J. Geophys. Res. B* **86**, 2593–2644.

Paukert A. N., Matter J. M., Kelemen P. B., Shock E. L. and Havig J. R. (2012) Reaction path modeling of enhanced *in situ* CO_2 mineralization for carbon sequestration in the peridotite of the Samail Ophiolite, Sultanate of Oman. *Chem. Geol.* **330–331**, 86–100.

Pentecost A. (2005) *Travertine*. Springer-Verlag, Berlin.

Power I. M., Wilson S. A., Thom J. M., Dipple G. M., Gabites J. E. and Southam G. (2009) The hydromagnesite playas of Atlin, British Columbia, Canada: A biogeochemical model for CO_2 sequestration. *Chem. Geol.* **260**, 286–300.

Power I. M., Wilson S. A., Small D. P., Dipple G. M., Wan W. and Southam G. (2011) Microbially mediated mineral carbonation: Roles of phototrophy and heterotrophy. *Environ. Sci. Technol.* **45**, 9061–9068.

Pronost J., Beaudoin G., Tremblay J., Larachi F., Duchesne J., Hébert R. and Constantin M. (2011) Carbon sequestration kinetic and storage capacity of ultramafic mining waste. *Environ. Sci. Technol.* **45**, 9413–9420.

Reimer P. J., Baillie M. G. L., Bard E., Bayliss A., Beck J. W., Blackwell P. G., Bronk Ramsey C., Buck C. E., Burr G. S., Edwards R. L., Friedrich M., Grootes P. M., Guilderson T. P., Hajdas I., Heaton T. J., Hogg A. G., Hughen K. A., Kaiser K. F., Kromer B., McCormac F. G., Manning S. W., Reimer R. W., Richards D. A., Southon J. R., Talamo S., Turney C. S. M., van der Plicht J. and Weyhenmeyer C. E. (2009) INTCAL09 and MARINE09 radiocarbon age calibration curves, 0–50,000 years cal BP. *Radiocarbon* **51**, 1111–1150.

Roberts M. L., Burton J. R., Elder K. L., Longworth B. E., McIntyre C. P., von Reden K. F., Han B. X., Rosenheim B. E., Jenkins W. J., Galutschek E. and McNichol A. P. (2009) A high performance 14-C accelerator mass spectrometry system. Proceedings of the 20th International Radiocarbon Conference, Radiocarbon, Kona, HI (abstr.).

Rozanski K., Stichler W., Gonfiantini R., Scott E. M., Beukens R. P., Kromer B. and van der Plicht J. (1992) The IAEA C-14 intercomparison exercise 1990. *Radiocarbon* **34**, 506–519.

Schauble E. A., Ghosh P. and Eiler J. M. (2006) Preferential formation of 13C–18O bonds in carbonate minerals, estimated using first-principles lattice dynamics. *Geochim. Cosmochim. Acta* **70**, 2510–2529.

Scott E. M. (2003) The third international radiocarbon intercomparison (TIRI) and the fourth international radiocarbon intercomparison (FIRI) 1990–2002. Results, analyses, and conclusions. *Radiocarbon* **45**, 135–408.

Searle M. P. and Cox J. (1999) Tectonic setting, origin, and obduction of the Oman ophiolite. *Geol. Soc. Amer. Bull.* **111**, 104–122.

Searle M. P. and Cox J. (2002) Subduction zone metamorphism during formation and emplacement of the Semail ophiolite in the Oman Mountains. *Geol. Mag.* **139**, 241–255.

Seifritz W. (1990) CO_2 disposal by means of silicates. *Nature* **345**, 486.

Staudigel H., Hart S. R., Schmincke H.-U. and Smith B. M. (1989) Cretaceous ocean crust at DSDP Sites 417 and 418: Carbon uptake from weathering verses loss by magmatic outgassing. *Geochim. Cosmochim. Acta* **53**, 3091–3094.

Stephen A. L., Jenkin G. R. T., Styles M. T., Smith D. J., Naden J., Boyce A. J., Leng M. J. and Millar I. L. (2013) Tracing carbon: Mineral carbonation and the incorporation of atmospheric vs. recycled CO_2. *Energy Procedia* **37**, 5897–5904.

Streit E., Kelemen P. and Eiler J. (2012) Coexisting serpentine and quartz from the carbonate bearing serpentinized peridotite in the Samail Ophiolite, Oman. *Contrib. Mineral. Petrol.* **164**, 821–837.

Stuiver M. and Polach H. A. (1977) Discussion: Reporting of ^{14}C Data. *Radiocarbon* **19**, 355–363.

Stuiver M. (1980) Workshop on ^{14}C data reporting. *Radiocarbon* **22**, 964–966.

Surour A. A. and Arafa E. H. (1997) Ophicarbonates: Calichified serpentinites from Gebel Mohagara, Wadi Ghadir area, Eastern Desert, Egypt. *J. Afr. Earth Sci.* **24**, 315–324.

Trommsdorff V. and Evans B. W. (1977) Antigorite-ophicarbonates: Contact metamorphism in Valmalenco, Italy. *Contrib. Mineral. Petrol.* **62**, 301–312.

Trommsdorff V., Evans B. W. and Pfeifer H. R. (1980) Ophicarbonate rocks: Metamorphic reactions and a possible origin. *Arch. Sci. Genève* **33**, 361–364.

Vadpalas B., Weidman C. and Cronin E. K. (2011) Validation of age estimation in geoduck clams using the bomb radiocarbon signal. *J. Shellfish Res.* **30**, 1–5.

Vogel J. S., Nelson D. E. and Southon J. R. (1987) ^{14}C background levels in an accelerator mass spectrometry system. *Radiocarbon* **29**, 323–333.

Weyhenmeyer C. E. (2000) Origin and evolution of groundwater in the alluvial aquifer of the eastern Batinah coastal plain, Sultanate of Oman: A hydrogeological approach. Ph. D. thesis, Univ. Bern, Switzerland.

Wilson S. A., Raudseep M. and Dipple G. M. (2006) Verifying and quantifying carbon fixation in minerals from serpentine-rich mine tailings using the Rietveld method with X-ray powder diffraction data. *Am. Mineral.* **91**, 1331–1341.

Wilson S. A., Raudsepp M. and Dipple G. M. (2009a) Quantifying carbon fixation in trace minerals from processed kimberlite: A comparative study of quantitative methods using X-ray powder diffraction data with applications to the Diavik Diamond Mine, Northwest Territories, Canada. *Appl. Geochem.* **24**, 95–112.

Wilson S. A., Dipple G. M., Power I. M., Thom J. M., Anderson R. G., Raudsepp M., Gabites J. E. and Southam G. (2009b) Carbon dioxide fixation within mine wastes of ultramafic hosted ore deposits: Examples from the Clinton Creek and Cassiar chrysotile deposits, Canada. *Econ. Geol.* **104**, 95–112.

Wilson S. A., Barker S. L. L., Dipple G. M. and Atudorei V. (2010) Isotopic disequilibrium during uptake of atmospheric CO_2 into mine process waters: Implications for CO_2 sequestration. *Environ. Sci. Technol.* **44**, 9522–9529.

Xu X. M., Trumbore S. E., Zheng S. H., Southon J. R., McDuffee K. E., Luttgen M. and Liu J. C. (2007) Modifying a sealed tube zinc reduction method for preparation of AMS graphite targets: Reducing background and attaining high precision. *Nucl. Instrum. Meth. B* **259**, 320–329.

Associate editor: F. McDermott